Stockholm University

Collision Induced Fragmentation of Molecules and Molecular Clusters

Knockout Driven Reactions in Fullerenes and PAHs

Michael Gatchell

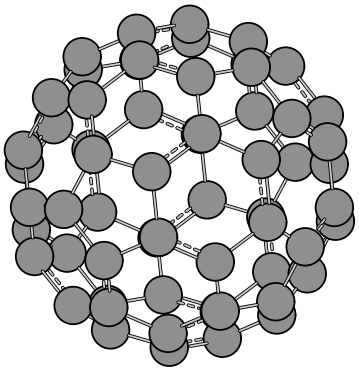

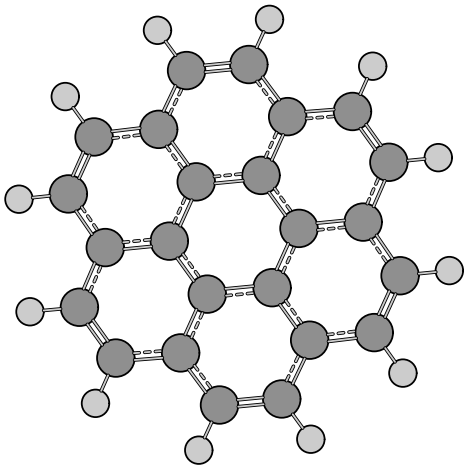

Abstract

This licentiate thesis covers experimental and theoretical studies of the fragmentation and subsequent reactions of fullerenes or Polycyclic Aromatic Hydrocarbons (PAHs). I present results from experiments where atoms or ions collide with fullerenes, PAHs, or clusters of these molecules at energies from 100 eV up to tens of keV.

The results of these experiments are interpreted using quantum chemical calculations, molecular dynamics simulations, and a stopping model that we have developed. With these models I show that different energy transfer processes dominate at different collision energies, from nuclear stopping in low energy ($\sim$ 100 eV) collisions to electronic stopping at higher energies ($\sim$ 10 keV). I particularly focus on non-statistical fragmentation induced by nuclear stopping which can lead to the formation of exotic new species such as the odd-numbered C_{119} fullerene-like molecule.

©Michael Gatchell, Stockholm 2014

Printed in Sweden, Stockholm 2014

Distributor: Department of Physics, Stockholm University

To Ea

List of Papers

The following papers, referred to in the text by their Roman numerals, are included in this thesis.

PAPER I: **Non-statistical fragmentation of PAHs and fullerenes in collisions with atoms**
M. Gatchell, M. H. Stockett, P. Rousseau, T. Chen, K. Kulyk, H. T. Schmidt, J. Y. Chesnel, A. Domaracka, A. Méry, S. Maclot, L. Adoui, K. Støchkel, P. Hvelplund, Y. Wang, M. Alcamí, B. A. Huber, F. Martín, H. Zettergren and H. Cederquist, *International Journal of Mass Spectrometry*, in press (2014).
DOI: 10.1016/j.ijms.2013.12.013

PAPER II: **Nonstatistical fragmentation of large molecules**
M. H. Stockett, H. Zettergren, L. Adoui, J. D. Alexander, U. Bērziņš, T. Chen, M. Gatchell, N. Haag, B. A. Huber, P. Hvelplund, A. Johansson, H. A. B. Johansson, K.Kulyk, S. Rosén, P. Rousseau, K. Støchkel, H. T. Schmidt and H. Cederquist, *Physical Review A*, **89**, 032701 (2014).
DOI: 10.1103/PhysRevA.89.032701

PAPER III: **Formations of Dumbbell C_{118} and C_{119} inside Clusters of C_{60} Molecules by Collision with α Particles**
H. Zettergren, P. Rousseau, Y. Wang, F. Seitz, T. Chen, M. Gatchell, J. D. Alexander, M. H. Stockett, J. Rangama, J. Y. Chesnel, M. Capron, J. C. Poully, A. Domaracka, A. Méry, S. Maclot, H. T. Schmidt, L. Adoui, M. Alcamí, A. G. G. M. Tielens, F. Martín, B. A. Huber, and H. Cederquist, *Physical Review Letters*, **110**, 185591 (2013).
DOI: 10.1103/PhysRevLett.110.185501

PAPER IV: **Ions colliding with clusters of fullerenes - Decay pathways and covalent bond formations**
F. Seitz, H. Zettergren, P. Rousseau, Y. Wang, T. Chen, M. Gatchell, J. D. Alexander, M. H. Stockett, J. Rangama, J. Y. Chesnel, M. Capron, J. C. Poully, A. Domaracka, A. Meéry, S. Maclot, V. Vizcaino, H. T. Schmidt, L. Adoui, M. Alcamií, A. G. G. M. Tielens, F. Martín, B. A. Huber, and H. Cederquist, *The Journal of Chemical Physics*, **139**, 034309 (2013).
DOI: 10.1063/1.4812790

PAPER V: **Ions colliding with polycyclic aromatic hydrocarbon clusters**
M. Gatchell, H. Zettergren, F. Seitz, T. Chen, J. D. Alexander, M. H. Stockett, H. T. Schmidt, A. Ławicki, J. Rangama, P. Rousseau, M. Capron, S. Maclot, R.

Maisonny, A. Domaracka, L. Adoui, A. Méry, J.-Y. Chesnel, B. Manil, B. A. Huber and H. Cederquist, *Physica Scripta*, **T156**, 014062 (2013).
DOI: doi:10.1088/0031-8949/2013/T156/014062

PAPER VI: **Ions colliding with mixed clusters of C_{60} and Coronene**
M. Gatchell, M. H. Stockett, P. Rousseau, T. Chen, K. Kulyk, H. T. Schmidt, J. Y. Chesnel, A. Domaracka, A. Méry, S. Maclot, L. Adoui, B. A. Huber, H. Zettergren and H. Cederquist, *Physical Review A*, submitted (2014).

PAPER VII: **Absolute fragmentation cross sections in atom-molecule collisions: Scaling laws for non-statistical fragmentation of PAH molecules**
T. Chen, M. Gatchell, M. H. Stockett, J. D. Alexander, Y. Zhang, P. Rousseau, A. Domaracka, S. Maclot, R. Delaunay, L. Adoui, B. A. Huber, T. Schlathölter, H. T. Schmidt, H. Cederquist and H. Zettergren, *Journal of Chemical Physics*, submitted (2014).

PAPER VIII: **First storage of ion beams in the Double Electrostatic Ion-Ring Experiment: DESIREE**
H. T. Schmidt, R. D. Thomas, M. Gatchell, S. Rosén, P. Reinhed, P. Löfgren, L. Braännholm, M. Blom, M. Björkhage, E. Bäckström, J. D. Alexander, S. Leontein, D. Hanstorp, H. Zettergren, L. Liljeby, A. Källberg, A. Simonsson, F. Hellberg, S. Mannervik, M. Larsson, W. D. Geppert, K. G. Rensfelt, H. Danared, A. Paál, M. Masuda, P. Halldén, G. Andler, M. H. Stockett, T. Chen, G. Källersjö, J. Weimer, K. Hansen, H. Hartman, and H. Cederquist, *Review of Scientific Instruments*, **84**, 055115 (2013).
DOI: 10.1063/1.4807702

PAPER IX: **Commissioning of the DESIREE storage rings - a new facility for cold ion-ion collisions**
M. Gatchell, H. T. Schmidt, R. D. Thomas, S. Rosén, P. Reinhed, P. Löfgren, L. Braännholm, M. Blom, M. Björkhage, E. Bäckström, J. D. Alexander, S. Leontein, D. Hanstorp, H. Zettergren, L. Liljeby, A. Källberg, A. Simonsson, F. Hellberg, S. Mannervik, M. Larsson, W. D. Geppert, K. G. Rensfelt, H. Danared, A. Paál, M. Masuda, P. Halldén, G. Andler, M. H. Stockett, T. Chen, G. Källersjö, J. Weimer, K. Hansen, H. Hartman, and H. Cederquist, *Journal of Physics: Conference Series*, **488**, 012040 (2014).
DOI: 10.1088/1742-6596/488/1/012040

Reprints were made with permission from the publishers.

Author's contribution

The work presented in this thesis covers experimental work carried out at the Department of Physics at Stockholm University as well as at the CIMAP laboratory in Caen, France. For the work performed in France (parts of Paper I and Papers III, IV, V and VI), I took part in the planning and operation of the experiments. This involved a total of four weeks of beam time at the CIMAP lab. I have performed data analysis for Papers I, II, III, IV, V, VI, VII, VIII and IX. I am part of the group of people who have built and operate the ISLAB beam line at Stockholm University which was used for the experiments reported in Papers I and II. I ran the experiment and performed all of the data analysis during the early commissioning of the DESIREE ion storage ring facility (Papers VIII and IX).

Alongside of the experimental work described above, I also play an active role in constructing the theoretical models used to aid the interpretations. For Papers IV and V I wrote the simulation software which was used to model the cluster evaporation processes. For Paper VII I performed the quantum chemical calculations used to study the increased reactivity of defect PAH molecules. More recently I have developed molecular dynamics simulations to model collisions between keV ions and fullerene or PAH molecules and the subsequent reactions that can occur when these systems are parts of clusters (Papers I and VI).

Contents

Abstract **ii**

List of Papers **v**

Author's contribution **vii**

1 Introduction **11**

2 Experimental Details **13**
2.1 Atomic Ions Colliding with PAHs and Fullerenes 13
2.1.1 Monomer and Cluster Sources for PAHs and Fullerenes 13
2.1.2 Time-of-Flight Mass Spectrometer 14
2.1.3 Data Analysis 16
2.2 PAH and Fullerene Ions Colliding with Noble Gas Atoms 16

3 Theoretical Methods **19**
3.1 The Quantum Approach 19
3.1.1 Density Functional Theory 20
3.2 The Classical Approach 20
3.2.1 The Tersoff Potential 22
3.2.2 Simulating Molecular Interactions 23
3.3 Energy Transfer in Collisions: Electronic and Nuclear Stopping 24
3.3.1 Modeling Electronic Stopping 25
3.3.2 Modeling Nuclear Stopping 26

4 Results and Discussion **29**
4.1 Electronic and Nuclear Stopping 29
4.2 Statistical vs. Non-statistical Fragmentation 29
4.2.1 Isolated Molecules 29
4.2.2 Molecular Clusters 32
4.3 Knockout Induced Chemistry 34

5 Summary and Outlook **39**

Additional Publications **xli**

1. Introduction

Carbon forms the backbone for all organic chemistry and is a main building block in e.g. proteins, nucleic acids and lipids. The reason for this is the carbon atom's valence electron structure, with four vacancies, allows carbon to form countless molecular structures with other carbon atoms or with other atomic species. Molecules containing carbon are not only abundant on earth; a majority of the over 170 molecules spectroscopically identified in space [1] contain carbon, and all but one of those with more than four atoms are organic [2].

A family of particularly stable carbonaceous molecules are the Polycyclic Aromatic Hydrocarbons or PAHs for short. They typically have planar ring-based structures (see fig. 1.1 for two examples) often with six carbon atoms per ring. These aromatic rings give an increased stability due to their delocalized molecular orbitals. In the 1980's, PAHs were proposed [3] as the origin of the unidentified infrared (IR) spectral features (see Ref. [4] for a recent review of astronomical PAHs). PAHs are identified in astronomical spectra by their strong emission in the mid-IR, due to transitions between different vibrational states [5]. The corresponding vibrational frequencies differ only slightly between different PAH species, and thus it is currently impossible to uniquely identify individual PAH species in space, but typical interstellar PAHs are expected to contain at least 50-100 carbon atoms [6]. Clusters of PAHs are believed to be one of the building blocks of interstellar dust [6–8], which plays an important role in stellar and planetary formation [9].

Molecular structures containing only one atomic species, but which differ in molecular crystalline structure, are known as allotropes. Carbon is known to have at least three allotropes: graphite, diamond and fullerenes. The first two types have been known since antiquity. Fullerenes on the other hand were first discovered in 1985 in an experiment where graphite was vaporized by a laser [10]. This resulted in the formation of a highly stable C_{60} structure (left in fig. 1.1), a closed spherical cage of 60 carbon atoms in a mixed hexagonal and pentagonal pattern (20 hexagons and 12 pentagons in C_{60}). The geometrical structure of C_{60} is identical to that of a classic soccer ball. Fullerenes (C_{60} and C_{70}) have also been identified in the same astrophysical regions as PAHs [11–14] and are currently the largest molecules that have been observed in space [1].

The exact origins of PAHs and fullerenes in space remain unknown. In spite of the fact that fullerenes, PAHs and related molecules are estimated to contain at least 5 and perhaps up to 20 percent of the cosmic carbon [15, 16], many questions regarding these molecules still remain unanswered: How are they formed? How do they grow? How do they survive in harsh environments? The key to answering these questions is through lab experiments and theoretical models. There are several models used to describe various growth mechanisms of PAHs [17] and fullerenes [15, 18, 19]. An additional aspect is also the link between the PAHs and fullerenes, where it has been suggested that large PAHs may be processed to form closed fullerene cages through the formation of pentagonal rings which give a curved molecular structure [15, 19].

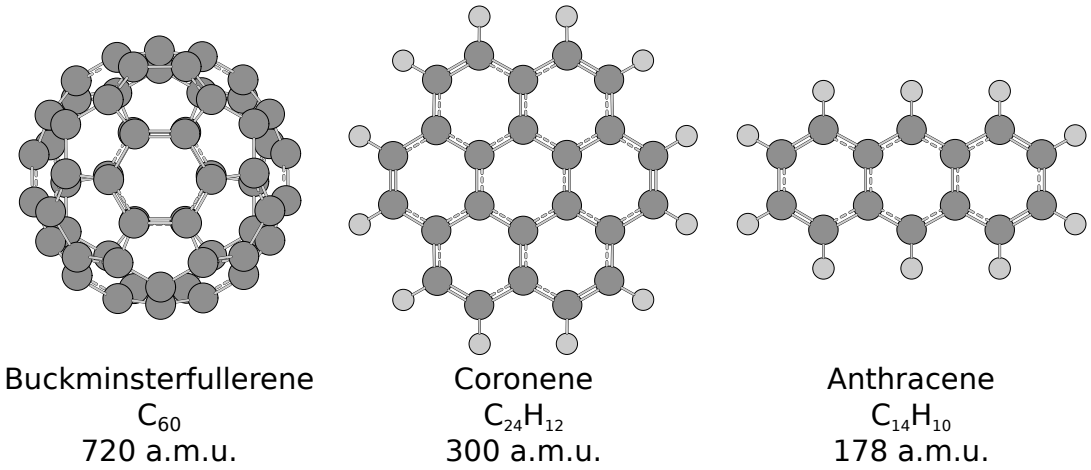

Figure 1.1: Examples of a fullerene structure, C_{60}, and two PAH structures, coronene and coronene.

Evolution of these stable molecules is driven by the input of energy, exciting the molecules and overcoming reaction barriers. This can be studied in a number of different ways – through photoabsorbtion [20–25] or collisions with electrons [26], ions [27–34], or atoms [35, 36]. The stable structures and high level of symmetry of PAHs and fullerenes make these suitable prototypes for studying fragmentation processes which may otherwise be difficult to untangle in more complex molecular systems.

In this thesis I present and discuss results for atoms (or atomic ions) colliding with PAHs and fullerenes. We have performed studies of these molecules, both when they are isolated in vacuum and when they are parts of larger clusters, at center-of-mass energies from about 100 eV up to several tens of keV. This energy range is typical of that found in winds of ionized particles emitted from stars and supernovae [37, 38]. The experimental results are interpreted with the aid of theoretical models. In the following summary, I will briefly discuss the main results of Papers I through IX. In addition, I will focus on a few additional key aspects which were not treated in full in these publications. In chapters 2 and 3, I will describe the experimental techniques and the model calculations in somewhat greater details than in the papers. The results are discussed in chapter 4, while chapter 5 is devoted to a summary and outlook.

2. Experimental Details

Two experimental setups have been used in Papers I, II, III, IV, V and VI. In the first experiment, atomic ions collide with neutral molecules or clusters of PAHs and/or fullerenes. In the second experiment, cations of PAHs or fullerenes collide with neutral noble gases. For a given center-of-mass collision energy, there are few differences between the processes studied in the two experiments for ions of low charge states – such as He^+ ions colliding with PAH molecules compared to PAH^+ ions colliding with neutral He atoms. The different findings in the two experiments are instead results of large differences in collision energies, where different mechanisms contribute to the energy transfer process.

2.1 Atomic Ions Colliding with PAHs and Fullerenes

The experiments presented in Papers I, III, IV, V and VI were performed at the ARIBE beamline, part of CIMAP (Centre de Recherche sur les Ions, les Matériaux et la Photonique) in Caen, France. Here [39], atomic ions are produced in an Electron Cyclotron Resonance (ECR) ion source and accelerated to keV energies, typically ~ 10 keV per charge. The continuous ECR ion beam is chopped in pulses of lengths of a few μs with a repetition rate a few kHz.

2.1.1 Monomer and Cluster Sources for PAHs and Fullerenes

Targets of gas phase molecular monomers are produced using an oven. We then use high purity powders ($\gtrsim 99\%$) of a single molecular species which are heated to bring the molecules into the gas phase (sublimation). For PAHs the temperature of the oven can be from room temperature for small molecules such as naphthalene ($C_{10}H_8$) or up to 200 °C in the case of larger molecules like coronene ($C_{24}H_{12}$). To sublimate C_{60} powder, temperatures of up to 600 °C are required. The temperature of the oven controls the rate of sublimation and thus the density of the molecular gas. We tune this to suit the experimental requirements. The oven has a small nozzle which limits the molecular flow into the region where it interacts with the ion beam.

We also produce weakly bound clusters of molecules. In the cluster source, an oven like the one which produces gas phase monomers, but operating at a higher temperature in order to give a high density of molecules, is placed in an enclosure with He buffer gas (fig. 2.1). The He gas, which is cooled with liquid N_2, cools the molecules from the oven so that they condense to form clusters. These clusters are weakly bound by dispersion forces and have broad, log-normal size distributions [40].

In experiments with mixed clusters of two molecular types (Paper VI), we use two ovens in the same enclosure. The oven temperatures are regulated independently depending on the types of molecules in order to get some control of the mixing ratios in the clusters.

The clusters, either containing a single molecular species or a mixture of two, escape through a small nozzle to the interaction region of the experiment.

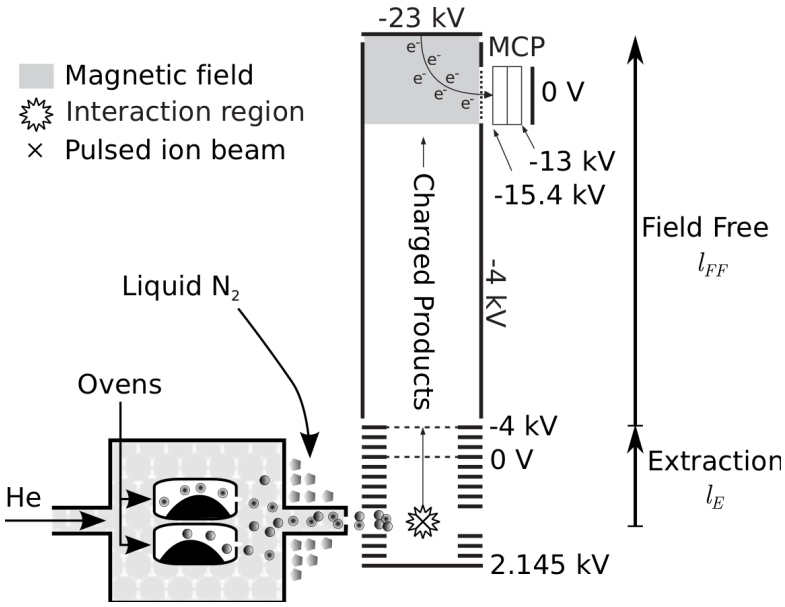

Figure 2.1: Schematic of the mixed cluster source and time-of-flight mass spectrometer. Mixed clusters are produced and enter the interaction region from the left in the figure. The pulsed ion beam enters, heading into the page, and collides with the neutral clusters at right angles. The mass-to-charge ratios of charged products are identified by their time-of-flight (c.f. text).

2.1.2 Time-of-Flight Mass Spectrometer

The pulsed keV ion beam collides with the neutral molecules or clusters in the interaction region of a linear time-of-flight mass spectrometer as shown in fig. 2.1. About 100 ns after the ion pulse has passed through the interaction region, an electrostatic potential V_E is applied. The extraction potential accelerates the charged products from the collision region of finite size to a kinetic energy which depends on the exact location of the collision point along the spectrometer axis. The further away from the end of the spectrometer they are produced the higher kinetic energy they obtain. The length of the field-free drift region is then adjusted so that the total flight time for the ions (from the switching of the extraction pulse to the ion impact on the metal plate) is independent to first order on where they were created inside the interaction region. The length of the Field Free region (FF) is $l_{FF} \approx 1$ m and it ends at a mesh after which the ions are accelerated by a strong field to a metal plate typically held at -23 kV. A shower of secondary electrons from the plate are guided to the Micro Channel Plate detector (MCP) by a weak magnetic field. The advantage of using a conversion plate instead of mounting the MCP detector directly at the end of the time-of-flight tube is that for each charged product that hits the metal plate, a large number of electrons are directed towards the MCP, ensuring a higher total detection efficiency [41]. The typical time-of-flight is up to a few hundred microseconds for masses corresponding to intact

molecules or clusters of PAHs and fullerenes and is measured with nanosecond resolution.

A simple derivation of the connection between the time-of-flight (t_{ToF}) and mass-per-charge (m/q) is as follows. As a first approximation we can assume that all charged products are produced at the same point and have zero kinetic energy. The extraction potential, V_E, accelerates the charged particles over a distance of $l_E = 11$ cm. The flight time in this region, t_E, is given by:

$$l_E = \frac{1}{2} a t_E^2 \tag{2.1}$$

$$\Rightarrow t_E^2 = \frac{2 l_E}{a} \quad \left\{ \text{where } a = \frac{q V_E}{m l_E} \right\} \tag{2.2}$$

$$\Rightarrow t_E^2 = \frac{2 l_E^2 m}{q V_E} \tag{2.3}$$

$$\Rightarrow t_E^2 \propto \frac{m}{q} \tag{2.4}$$

Since all of the charged products are accelerated to a constant kinetic energy (E_{kin}) and travel the same distance ($l_{FF} \approx 1$ m), the time-of-flight in the field free region, t_{FF}, is obtained through the following relations:

$$V_E = \frac{E_{kin}}{q} = \frac{m v_{FF}^2}{2q} \tag{2.5}$$

$$\Rightarrow \frac{m}{q} = \frac{2 V_E}{v_{FF}^2} = \frac{2 V_E t_{FF}^2}{l_{FF}^2} \tag{2.6}$$

$$\Rightarrow t_{FF}^2 \propto \frac{m}{q} \tag{2.7}$$

At the end of the field free region, the ions are again accelerated a short distance by the biased plate. The time-of-flight in this region, t_B, can be seen as the sum of two components, a free flight component with constant velocity (like in the field free region), and a component with constant acceleration (like in the extraction region). From eqs. (2.1)-(2.7) we can thus conclude that

$$t_B^2 \propto \frac{m}{q} \tag{2.8}$$

The total time-of-flight is then simply $t_{ToF} = t_E + t_{FF} + t_B$, which according to eqs. (2.4), (2.7) and (2.8) gives

$$\frac{m}{q} \propto t_{ToF}^2. \tag{2.9}$$

An additional piece of information which may be obtained from the time-of-flight measurement is the kinetic energy of the charged particles following the initial collision and possible subsequent fragmentation steps. This leads to a broadening of the time-of-flight peak profile. Based on the width of the line profiles we are able to determine the typical kinetic energies of the detected particles at the time when the extraction pulse was applied [42].

2.1.3 Data Analysis

In the previous section, I showed that the mass-per-charge of a charged product is proportional to the time-of-flight squared. This is true in the ideal case, but not necessarily in the real experiment. Instead of using a simple power law as in the ideal case, we use a polynomial, of at least second order, to convert the measured time-of-flight into the more useful unit of mass-per-charge. This compensates for imperfections in the measurements.

A benefit of using the time-of-flight mass spectrometer is the ability to study correlations between several charged fragments from single collision events. In these so called *coincidence measurements*, the ion beam intensity and/or the target thickness are down-tuned so that the probability of there being more than one collision per beam pulse is negligible. If this is the case, then all charged products from a single ion pulse interacting with the target come from a single collision. We use this information to get a clearer picture of the processes involved in the dissociation of molecules or clusters.

2.2 PAH and Fullerene Ions Colliding with Noble Gas Atoms

Experiments involving collisions between PAH or fullerene ions and a neutral gas target (Papers I and II) were performed at Stockholm University. Here we have built an electrospray ion source in the so-called ISLAB (Ion Source LAB) which is an essential part of the Double ElectroStatic Ion Ring ExpEriment (DESIREE) facility (Papers VIII and IX and [43]). The ISLAB setup (fig. 2.2) is currently being used for standalone experiments.

Electrospray ionization is a relatively gentle method for producing ions and is frequently used for ionizing fragile systems such as bio-molecules [44] and gets its name from the way ions are produced. The molecules that are to be ionized are dissolved and the solution is fed by a syringe into a needle which is held at high voltage, usually a few kV. Opposite to the needle tip is a heated capillary which is the entrance to the beam line. Droplets formed at the needle are charged by the high voltage and enter the capillary. The heat from the capillary enhances the evaporation of the droplets, increasing the charge density of the droplets until they Coulomb explode, eventually resulting in the bare ions.

The ions are steered through the apparatus by a series of octupole beam guides and Einzel lenses. We use a quadrupole mass filter to select the desired ion mass and ensure a beam with a well defined mass-to-charge ratio. The ion beam is then accelerated by a potential of up to energies between 1 and 10 keV. The keV ions enter a gas cell through a small opening where they can collide with a gas target at a well defined pressure measured with a capacitance manometer (a Baratron). The kinetic energy of charged products from the collisions are identified using a series of electrostatic deflector plates or a hemispherical analyzer and an MCP detector.

We use this experiment to ionize PAH or fullerene molecules, accelerate them to up to 10 keV, and collide them with noble gas atoms. This experimental setup operates essentially in the opposite way to the experiments described in section 2.1. Now the charged PAH and fullerene molecules are accelerated. The main results of this distinction is the difference in collision velocities in the experiments in Stockholm and in Caen. The lab frame kinetic energies in the two experiments are similar (about 10 keV per charge), but when we accelerate the much heavier

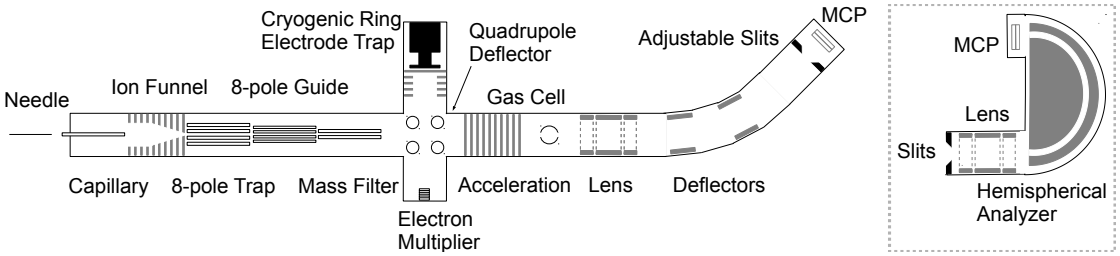

Figure 2.2: Schematic of the experimental setups used in ISLAB. A solution is injected through a charged needle from the left. The charged droplets evaporate and Coulomb explode in the capillary leaving bare ions. The ions are guided to the quadrupole mass filter where we mass select the ion of interest. We then accelerate the ion beam towards the gas cell towards the right. After the collisions, the ion beam is analyzed using either deflecting plates or a hemispherical analyzer (inset) and an MCP detector. The trapping and cooling of ions is not in use in the experiments presented here.

molecules instead of the atomic ions we get collisions with much lower energies in the center-of-mass reference frame. For further descriptions of the experimental procedure please refer to Papers I and II.

3. Theoretical Methods

We use theoretical models to aid the interpretations of the experimental results. Here we have used classical Molecular Dynamics simulations to study some of the molecular fragmentation processes and molecular reactivities inside clusters. We have further used Density Functional Theory to study stabilities and possible further decays of fragments and reactivities with other atomic or molecular species. These topics and methods make up a whole field of science of its own and below follows a short description of methods used in the Papers in this thesis.

3.1 The Quantum Approach

Quantum mechanics is required to fully describe the electronic structure of an atom or molecule. The development of quantum mechanics over the last hundred years has vastly increased our understanding of the nature of atoms, molecules, their interactions, the properties of various types of materials etc.

Much like classical mechanics, it is rather straightforward to analytically calculate the motion of an interacting two body system over time. A classical example of this is predicting the orbit of the moon around the earth. The quantum mechanical equivalent to this problem is the hydrogen atom, with a single electron interacting with a single proton. To solve this problem we solve the Schödinger equation

$$i\hbar\frac{\partial\Psi}{\partial t} = H\Psi \tag{3.1}$$

where Ψ is the wave function which describes the system and $H = T + V$ is the Hamiltonian operator, where T and V are operators relating to the kinetic and potential energy of the system, respectively. The potential energy operator in this case is simply the attraction due to the Coulomb interaction between the electron and the proton. The calculation is usually simplified further by assuming that the motion of the proton and the electron are decoupled, e.g. that the electron moves around a stationary nucleus.

While solving the Schödinger equation for the hydrogen atom is a rather simple endeavor, done in most introductory courses in quantum mechanics, there is no closed-form solution for any other neutral atom or molecule (i.e. any system with more than one electron or more than one nucleus). The problem is to find solutions to a quantum mechanical many-body system, something that is not possible to do analytically for exact solutions.

Using the Hartree-Fock (HF) method with its simplifying assumptions, approximate solutions to the Schrödinger equation may be found even for atoms and molecules with many electrons. For molecules the Born-Oppenheimer approximation is essential as we may then separate the nuclear and electronic degrees of freedom when solving the problem. We may thus solve for

the electronic wavefunction with the nuclei in the molecule assumed to be fixed in space. This is quite reasonable as the "orbiting times" of electrons in atoms or molecules are in the attosecond range (10^{-18} s) while typical vibrational timescales in molecules are picoseconds (10^{-12} s).

The main limiting simplification in the HF method for a system near equilibrium is the mean field approximation in which interactions between individual pairs of electrons are treated in an average fashion. Due to the lack of electron correlation in the HF method, the total electron energy in the HF method is, for a given Hamiltonian, always above the "real" energy of a system, where all correlation and a complete set of basis functions are included. A wide range of so-called post-HF methods have been developed to bridge this gap. Different approaches can be used to include different types of electron correlation, all increasing the computational power needed.

3.1.1 Density Functional Theory

An alternative to HF-based methods is Density Functional Theory (DFT) [45]. In DFT, one uses the electron density to determine the energy of a system, in contrast to the wave-functions based HF method. This is possible due to the Hohenberg-Kohn theorem [46] which states that there is a direct one-to-one correspondence between the unique ground state n-body wave function ($\Psi_0(\mathbf{r}_1, \mathbf{r}_2, \ldots, \mathbf{r}_n)$) and the ground state electron density ($n_0(\mathbf{r})$) of a system. This means that the problem of solving the n-body Schödinger equation is reduced to solving a problem only dependent on the three spatial coordinates ($\mathbf{r} = (x, y, z)$). There is a catch to this scheme though, while many of the components of the DFT method are well-defined, the exact functional describing the exchange-correlation energy is unknown. The approach (functional) used to describe exchange-correlation energy is what sets different DFT methods apart. A plethora of different DFT functionals exist, from purely theoretical models to empirically fitted forms and anything in between. Functionals used in the papers in this thesis include B3LYP [47], the "standard" DFT functional for isolated molecular systems, as well as ωB97XD [48] and M06-L [49] functionals which better describe dispersion forces which are crucial in loosely bound systems such as clusters [50].

DFT offers a method for including electron correlation in quantum chemical calculations at a computational cost similar to that of the HF method. Yet the computational resources required are still significant for large systems. As an example, the optimization of the ground-state mixed C_{60}-coronene dimer structure, a system with 96 atoms and 516 electrons, took 111 days to converge on a modern 4-core desktop computer using the relatively small 6-31+G(d) basis set and the ωB97XD functional. We clearly need another approach to study the dynamics of such systems.

3.2 The Classical Approach

When a problem is too large to be solved using quantum chemical methods in a reasonable amount of time, an option is to use classical Molecular Dynamics (MD) simulations. In MD simulations, the electronic structure of molecules are neglected entirely and each molecular bond is instead described using a model force field. The general form of the energy in such a

force field is given by the following expression.

$$E = E_{\text{bond}}(r_{ij}) + E_{\text{angle}}(\theta_{ijk}) + E_{\text{dihedral}}(\varphi_{ijkl}) + E_{\text{non-bonded}} \tag{3.2}$$

Here, $E_{\text{bond}}(r_{ij})$ is the potential energy of a linear bond between two atoms, $E_{\text{angle}}(\theta_{ijk})$ the potential energy from the distortion of an angle between three atoms, $E_{\text{dihedral}}(\varphi_{ijkl})$ the potential from the bending of the dihedral angle in a four atom structure, and $E_{\text{non-bonded}}$ is the potential energy from interactions between atoms which are not directly bonded. When modeling molecular systems, potentials that reproduce the physical characteristics of the system are chosen. This can be done by choosing a potential which has the correct shape and binding energy between atoms and ensures that the ground state structure is correct. As an example, a simple model of a single water molecule is shown in fig. 3.1. The water molecule has two O-H bonds which are separated by the angle $\theta_{12} = 104.5°$. The potential for describing such a planar molecule with two bonds thus contains three terms

$$E = E_{r_1} + E_{r_2} + E_{\theta_{12}} \tag{3.3}$$

and is minimized when the structure is relaxed.

Selecting potentials which give the correct behavior of these energies can be done by fitting experimental results or using higher levels of theory, such as quantum chemical methods. One major advantage of using classical MD models is the ability to simulate the time evolution of very large systems such as liquids or crystals. In these cases, potentials which give a poor or even incorrect description of single molecules may be still be preferential if it gives a good description of the bulk substance.

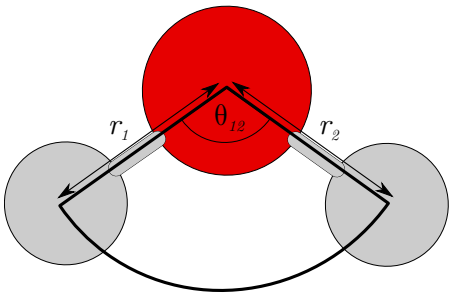

Figure 3.1: The water molecule can be described using two O-H bonds with lengths r_1 and r_2 separated by the angle θ_{12}.

The general procedure for an MD simulations is as follows:

1. The structure being studied is defined, that is, the position of every simulated atom is defined by coordinates in space.

2. Potentials describing the interactions between atoms are defined. Multiple potentials can be used simultaneously to describe different types of interactions.

3. Calculate the net force vector acting on each atom in the system.

4. Solve the equations of motion for each atom and follow the trajectories for a small time step.

5. Repeat steps 3 and 4 as long as desired.

3.2.1 The Tersoff Potential

For the simulations presented in Papers III and VI, we use the Tersoff reactive bond order potential [51, 52] to describe the bonds in fullerene and PAH molecules. A bond order potential differs somewhat from the picture described above where each bond and angle is describe independently. Here, the environment near each atom is considered when determining the potential energy surface of the system. This allows reactions, where bonds are formed or broken, to be modeled without the bonds being explicitly defined for each atom pair. Following the notation used by Tersoff [52], the potential energy is defined as the sum of the energies of each atom E_i, or equivalently as a sum over the energy stored in each binary bond V_{ij}.

$$E = \sum_i E_i = \frac{1}{2}\sum_{i \neq j} V_{ij} \tag{3.4}$$

$$V_{ij} = f_C(r_{ij})[f_R(r_{ij}) + b_{ij} f_A(r_{ij})] \tag{3.5}$$

The potential energy of each bond contains two exponential components, f_R which models the repulsive (R) component of the bond and f_A which describes the attractive (A) part of the potential. The choice of two exponential profiles give an overall Morse type potential, a potential that is often used to describe diatomic bonds.

$$f_R(r_{ij}) = A_{ij}\exp(-\lambda_{ij} r_{ij}) \tag{3.6}$$

$$f_A(r_{ij}) = -B_{ij}\exp(-\mu_{ij} r_{ij}) \tag{3.7}$$

The potential in eq. (3.5) is cut off in an interval $R_{ij} < r_{ij} < S_{ij}$ using a smooth and continuous function f_C. This reduces the overall computational load by only including interactions between neighboring atoms.

$$f_C = \begin{cases} 1, & r_{ij} < R_{ij} \\ \frac{1}{2} + \frac{1}{2}\cos[\pi(r_{ij} - R_{ij})/(S_{ij} - R_{ij})], & R_{ij} < r_{ij} < S_{ij} \\ 0, & r_{ij} > S_{ij} \end{cases} \tag{3.8}$$

The Tersoff potential contains an essential so-called bond order term b_{ij} (see eq. (3.5)). This term ensures that binding energies weaken with increased coordination (number of bonding neighbors) in a realistic fashion.

$$b_{ij} = \chi_{ij}(1 + \beta_i^{n_i}\zeta_{ij}^{n_i})^{-1/2n_i} \tag{3.9}$$

$$\zeta_{ij} = \sum_{k \neq i,j} f_C(r_{ik})\omega_{ik} g(\theta_{ijk}) \tag{3.10}$$

$$g(\theta_{ijk}) = 1 + c_i^2/d_i^2 - c_i^2/[d_i^2 + (h_i - \cos\theta_{ijk})^2] \tag{3.11}$$

The term ζ_{ij} in the expression for b_{ij} (eq. (3.9)) can be seen as a sum over the nearest neighbors and includes the parameter $g(\theta_{ijk})$ which contains the angular dependence of the bond order of a given atom type (eq. (3.10)). Two mixing terms, χ_{ij} and ω_{ik} are used to fine tune the interplay of potential parameters in heteroatomic systems. For the systems studied here, we follow Tersoff [52] and only use the first mixing term, thus setting $\omega_{ik} = 1$.

The coefficients used in eqs. (3.4) to (3.11) are defined as

$$A_{ij} = (A_i A_j)^{1/2} \tag{3.12}$$
$$B_{ij} = (B_i B_j)^{1/2} \tag{3.13}$$
$$\lambda_{ij} = (\lambda_i + \lambda_j)/2 \tag{3.14}$$
$$\mu_{ij} = (\mu_i + \mu_j)/2 \tag{3.15}$$
$$R_{ij} = (R_i R_j)^{1/2} \tag{3.16}$$
$$S_{ij} = (S_i S_j)^{1/2} \tag{3.17}$$
$$\tag{3.18}$$

where X_i is the parameter X for the species of atom i. Numerical values of the parameters for different atom types which are used in the potential are obtained by fitting the model to other data. For our use, we find the appropriate parameters in the literature. The parameters used to model C- and H-atoms are presented in table 3.1 and are from ref. [52] and [53] respectively. For the mixing term χ_{C-H}, a value of 0.89 was chosen as this gave the best fit to the enthalpy of formation for a number of hydrocarbon molecules of different sizes from ref. [54].

Table 3.1: Parameters used in the Tersoff bond order potential for C and H atoms.

Parameter (Unit)	C	H
A (eV)	1.3936×10^3	87.7120
B (eV)	3.467×10^2	43.5310
λ (Å^{-1})	3.4879	3.7879
μ (Å^{-1})	2.2119	1.9800
β	1.5724×10^{-7}	4.0000
n	7.2751×10^{-1}	1.00
c	3.8049×10^4	0.00
d	4.384	1.00
h	-5.7058×10^{-1}	1.00
R (Å)	1.8	0.80
S (Å)	2.1	1.00
	$\chi_{C-H} = 0.89$	

3.2.2 Simulating Molecular Interactions

MD simulations of collisions between fullerene and/or PAH molecules or their fragments in Papers III and VI were done using the DL_POLY Classic software package [55]. The fullerene

and PAH molecules were modeled using DL_POLY's included module for the Tersoff potential with the parameters shown in table 3.1.

We simulated the collision between molecular pairs to study the reactions that can occur and the barriers involved. One case where this is useful is for fragmenting molecular clusters. When molecular clusters are heated and begin to fragment, the molecules gain some kinetic energy (typically up to about one eV for clusters of C_{60} and/or PAHs) and may collide with one another, which can induce bond formation. Usually, intra-cluster collision energies are too small to induce bond-forming between intact molecules (for example kinetic energies greater than 60 eV are required for C_{60} + $C_{60} \rightarrow C_{120}$ dumbbell formation [56]). But when an atom has been promptly removed from a molecule in a small impact parameter collision, with for instance a keV ion, the reaction barriers can decrease significantly.

Reactions between molecules and large fragments of C_{60} and coronene were modeled by first removing a single carbon atom from one of the intact molecules. This simulates the knockout process, which occurs on fs (10^{-15} s) timescales, much faster than the subsequent steps which occur on ps (10^{-12} s) timescales or longer. The positions and rotations of the two molecules are randomized such that their geometrical centers are separated by 10 Å along the z-axis. We work in the microcanonical ensemble (constant NVE) since, on the timescales studied (up to a few ps), the simulations are assumed to be adiabatic. The molecules are heated to 1000 K to simulate the heating of the system in the collision. This is done by randomly distributing energy among the degrees of freedom according to the thermal energy distribution. The result of the simulations presented here is not sensitive to the exact value of the assumed internal temperature up to at least 1000 K. The molecules are then given opposing velocities in the z-direction such that the intended center-of-mass collision energy is obtained while the total momentum of the system is zero. An example of the initial positions of a colliding C_{59} + $C_{24}H_{12}$ pair from Paper VI is shown in fig. 3.2. Following the collisions, the positions of all the 95 individual atoms in the two molecular systems are followed for up to a few tens of ps. From the separation of the geometric centers of the two molecules as a function of time it is possible to determine if bonds have formed between atoms belonging (initially) to different molecules.

3.3 Energy Transfer in Collisions: Electronic and Nuclear Stopping

When atoms and molecules collide, kinetic energy is transferred. The forces involved in the energy transfer are referred to as the stopping power. For collisions between atoms (including atoms in molecules) the total stopping power can be separated into two components, electronic stopping and nuclear stopping. The electronic stopping of an atom colliding with a molecule can be seen as the inelastic scattering of electrons in the collisions with the impacting projectile. This inelasticity leads to a slowing down of the projectile and the corresponding loss of kinetic energy is converted to electronic excitation energy. Nuclear stopping is a result of scattering of the colliding particles on the (screened) nuclei in the molecule. The screening of the nuclear charge by the electrons makes this a comparatively weak molecular heating process when the projectile passes all the nuclei in the molecule at large distances and with a high velocity. On the other hand, when the projectile passes one of the nuclei at a small distance and with a lower velocity it may transfer substantial amounts of energy to that particular nucleus. If the

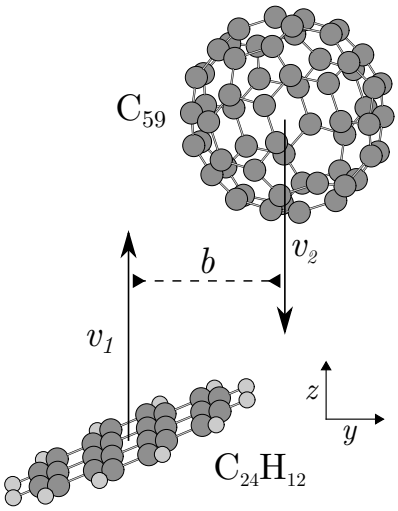

Figure 3.2: Example of initial positions in a simulation of a collision between C_{59} and $C_{24}H_{24}$ from Paper VI. The impact parameter b is defined as the separation in the xy-plane between the center-of-mass of the two molecules (here $b = 5$ Å).

energy is large enough that the corresponding atom may even leave the molecule carrying some kinetic energy with it. This will be discussed below in some detail as the knockout process which by definition is a non-statistical fragmentation process, i. e. there is no time to distribute the energy over the whole molecular system before the atom is ejected and fragmentation has already occurred.

We model the collisions using Monte Carlo methods to simulate random collision trajectories. The total energy transfer is then the sum of the electronic and nuclear stopping energies. The methods used to calculate these components are described in the following two sections.

3.3.1 Modeling Electronic Stopping

We model electronic stopping using formulae often used to model atom-solid collisions [29]. The picture we have here is that of an atom projectile colliding with a molecular target. The valence electrons of the molecular target are described as a free electron gas. The electron density as a function of position in the molecule is obtained from our DFT molecular structure calculations. From the local valence electron density n_0, the so called one-electron radius r_s can be defined,

$$r_s = \left(\frac{3}{4\pi n_0} \right)^{\frac{1}{3}}. \tag{3.19}$$

At the collision energies studied here, the electronic stopping energy is approximately proportional to the projectile velocity v [57] so that

$$\frac{dT_e}{dR} = \gamma(r_s)v \tag{3.20}$$

where $\gamma(r_s)$ is the friction coefficient which is connected to the scattering phase shifts (δ_l) of a partial wave expansion of a scattered electron through [58]

$$\gamma(r_s) = \frac{3}{k_F r_s^3} \sum_{l=0}^{\infty} (l+1) \sin^2(\delta_l - \delta_{l+1}). \tag{3.21}$$

Here k_F is the length of the Fermi wave vector, i.e. the radius of the Fermi sphere in momentum space. The friction coefficients for atoms embedded in a homogeneous electron gas at a few specific r_s values are available in the literature [58], but here we obtain γ for arbitrary values of r_s through a fitting procedure.

The electronic stopping energy of atoms (or atomic ions) colliding with molecules is calculated by following randomly chosen straight trajectories of the atom passing through the molecule's electron cloud. For each time step in the simulation, the local stopping power is calculated from eq. (3.20) and our fitted vaues for $\gamma(r_s)$. Multiplying the stopping power with the step length and summing over the entire path gives the total electronic stopping energy for a given collision trajectory.

3.3.2 Modeling Nuclear Stopping

Nuclear stopping power is the transfer of energy in short range interactions between the atomic nuclei. The interaction between the nuclei at very short ranges can be seen as the Coulomb interaction between two point charges corresponding to the nuclear charges. When the distance between the nuclei increases, the screening by the electrons decreases the effective strength of the scattering potential. A general form of the potential between two colliding atoms can thus be described by

$$V(r) = \frac{Z_1 Z_2}{r} f(x) \tag{3.22}$$

where Z_1 and Z_2 are the atomic number of the colliding atom pair and $f(x)$ is a screening function which goes to zero when $r \to \infty$ and one when $r = 0$. There are many different screening functions in the literature which are used for different types of interactions. In Paper VII we used the screened Bohr potential to obtain scaling laws for single atom knockout cross sections for PAHs. We have also used the ZBL (Ziegler, Biersack, Littmark) screening function, which is often used in ion-solid interactions, to model nuclear stopping. The ZBL-screening function is

$$f_{ZBL}(x) = 0.1818e^{-3.2x} + 0.5099e^{-0.9423x} + 0.2802e^{-0.4029x} + 0.02817e^{-0.2016x} \tag{3.23}$$

where

$$x = \frac{r}{a_{ZBL}} = \frac{r(Z_1^{0.23} + Z_2^{0.23})}{0.8853 a_0} \tag{3.24}$$

and a_{ZBL} is the so called screening length. The above functional form is a result of fitting the potential to the interactions between many different types of atomic pairs. The difference between the pure Coulomb potential and the potential using the ZBL screening function is shown in fig. 3.3.

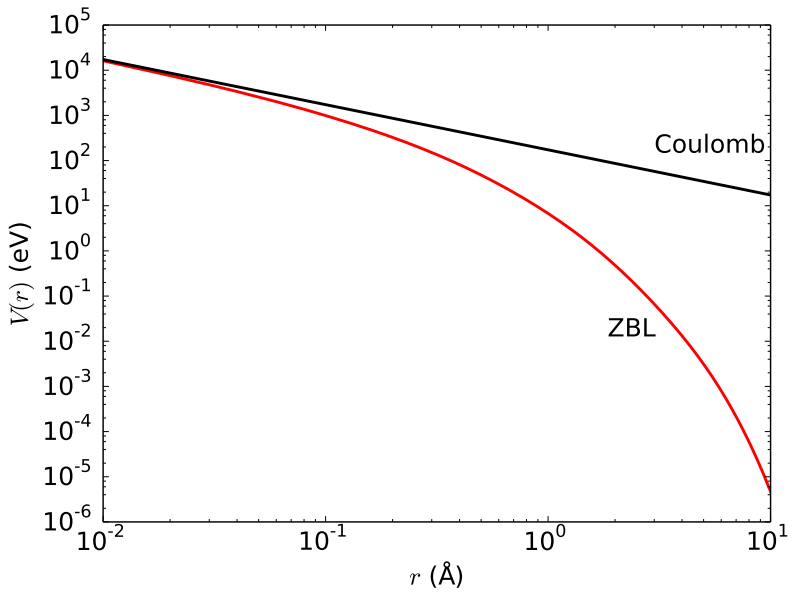

Figure 3.3: Potential energy as a function of separation between the nuclei of C and He atoms for the standard Coulomb potential and the ZBL screened potential. The ZBL screening function is a model for the screening of the two nuclei by the surrounding electrons and the two potentials are equal at $r = 0$.

The model used to calculate the nuclear stopping power in Papers II, III, IV, V and VII follow the same approach as for the electronic stopping. The stopping energy is calculated along a randomly chosen straight line trajectory through the molecule. For every trajectory we calculate both the electronic and nuclear stopping energy such that we get the total energy transfer for each individual trajectory.

Unlike the method used to model the electronic stopping described in section 3.3.1, the method we use to model the nuclear stopping can be fully included in classical MD simulations. We have implemented the ZBL screened Coulomb potential in DL_POLY. With this we can model the nuclear part of collisions between atoms and molecules. Early results from such MD simulations will be presented later in this thesis, but have so far not been included in any publications.

4. Results and Discussion

This section covers the results of Papers I, II, III, IV, V, VI and VII. I use the results from the stopping calculations to explain the observed differences between experiments at high (tens of keV) and low (up to 1 keV) center-of-mass collision energies. I present a simple model used to describe the fragmentation of molecular clusters. Finally, I discuss knockout induced chemical reactions in clusters of fullerene and/or PAH molecules.

4.1 Electronic and Nuclear Stopping

We have calculated the electronic and nuclear stopping energies for atoms colliding with a wide range of molecules at different collision energies using the method described in section 3.3 and Paper VII. In fig. 4.1 the electronic and nuclear stopping energy for He colliding with a coronene ($C_{24}H_{12}$) molecule face on at 110 eV and 11 keV center-of-mass energies are shown. We see immediately the short range nature of the nuclear stopping with energy transfer above a few eV being localized near the positions of the atoms in the molecule. In contrast we see that the electronic stopping is more evenly distributed and is particularly important in areas with high electron densities (e.g. bonds).

Typically the nuclear stopping dominates at low collision energies and electronic stopping at higher energies. This is indeed the case in the results shown in fig. 4.1. In the case of He colliding with coronene at a center-of-mass energy of 110 eV (top row in fig. 4.1), only the nuclear stopping energy exceeds 10 eV (in the face-on case) which is approximately where the small PAHs, e.g. anthracene ($C_{14}H_{10}$), start to fragment on the μs timescale of the experiment [59]. Thus we conclude that molecular fragmentation in such a collision is predominantly driven by nuclear stopping. At higher collision energies the nuclear stopping cross-section decreases while the electronic stopping energy increases strongly. In the case of He impacting on coronene with a center-of-mass energy of 11 keV, this results in the total stopping energy being dominated by the electronic stopping (lower row of fig. 4.1).

4.2 Statistical vs. Non-statistical Fragmentation

4.2.1 Isolated Molecules

When energy is deposited in a fullerene or PAH molecule or cluster, such as in a collision, it can be distributed among the internal modes of the system. If the system is heated strongly enough it may fragment as one of its ways to cool down. Alternative cooling mechanisms involve photo-emission and/or electron-emission processes. Isolated individual molecules may

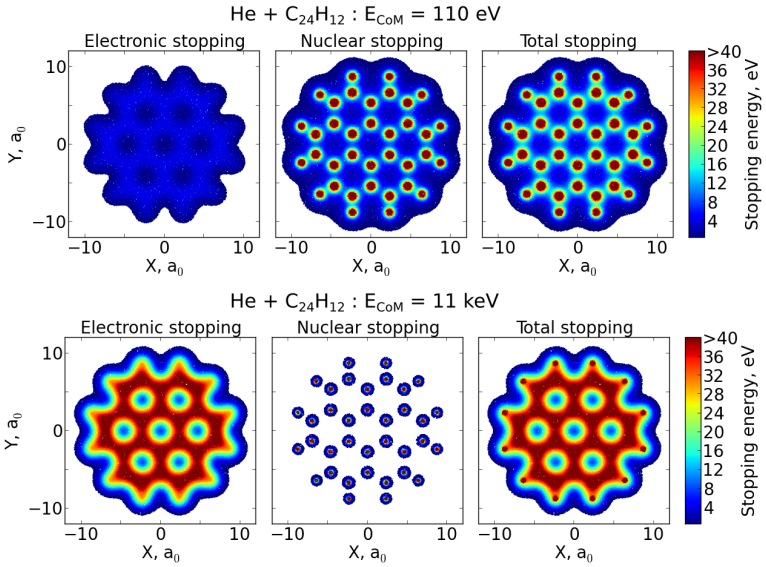

Figure 4.1: Electronic, nuclear and total stopping energies as functions of position for face-on collisions between He and coronene ($C_{24}H_{12}$) and center-of-mass energies of 110 eV (top row) and 11 keV (bottom row). At the lower collision energy the nuclear stopping energy dominates and at the higher energy the electronic stopping energy is dominant.

fragment by emitting atomic or molecular building blocks while clusters have an additional way of cooling through the emission of intact molecules. The fragmentation pathway taken in such processes is governed by the probability that a large enough fraction of the total internal energy is concentrated in a specific internal vibrational mode. The favored fragmentation pathway will then be the one with the lowest energy barrier. This type of fragmentation is known as *statistical fragmentation*. For fullerenes and PAHs, the statistically fragmenting molecules cool predominantly, as a first step, through the emission of C_2 ($\sim$ 10 eV dissociation energy [60]), or in the case of PAHs the loss of C_2H_2 or H ($\sim$ 5 eV dissociation energy for both mechanisms [61]).

An example of statistically driven fragmentation is shown in the lower panel of fig. 4.2 where He^+ ions collide with coronene molecules with a center-of-mass energy of 11 keV. As seen in fig. 4.1, most of the stopping energy in these collisions is from electronic excitation processes (electronic stopping). Initial steps of statistical fragmentation are observed as peaks corresponding to H- and C_2H_x-loss. Due to the large energy deposited in the coronene molecules, many of these initial fragments often decay further into smaller fragments which then give rise to the rather intense peaks at smaller mass-to-charge ratios in fig. 4.2.

In certain collisions, it is possible to induce fragmentation processes which are not the most energetically favorable. Such *non-statistical fragmentation* is observed in the experiments through the loss of a single carbon atom from a C_{60} or PAH molecule. This can be seen in the top panel of fig. 4.2 for He colliding with coronene cations at a center-of-mass kinetic energy of 110 eV. Now a peak in the mass spectrum comes from the loss of CH_x (11-17 eV dissociation

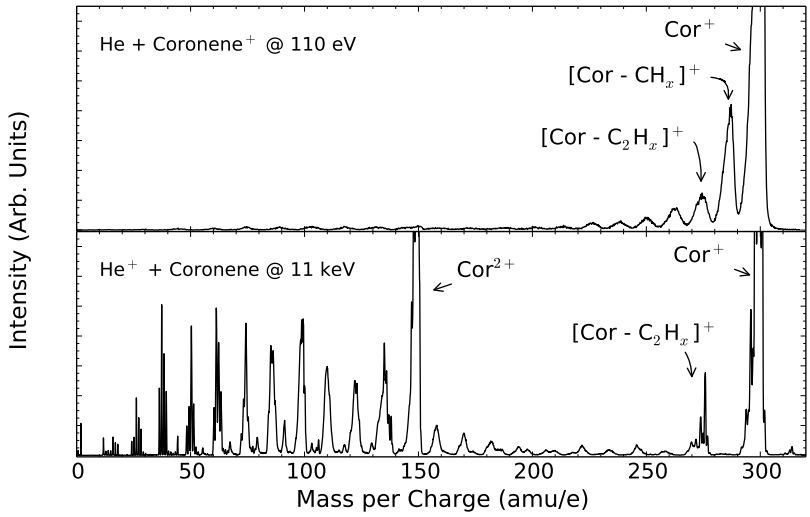

Figure 4.2: Mass spectra from collisions between He and coronene with center-of-mass energies of 110 eV (top panel) and 11 keV (bottom panel). The 110 eV mass spectrum has a strong feature from the loss of a single C-atom from coronene, a result of non-statistical fragmentation. This feature is absent from the higher collision energy spectrum which is dominated by statistical fragmentation.

energy depending on the initial position of the removed carbon atom), a process which is hard to explain using the statistical model and is strongly suppressed in the higher energy experiment (lower panel in fig. 4.2). This is instead a result of a prompt knockout of an atom in a small impact parameter collision (with respect to one C nucleus in the molecule). Here, nuclear stopping processes are dominant (compare with fig. 4.1). Such hard collisions deposit so much energy to individual atoms that they can be knocked out of the molecule before the energy can be dissipated throughout the molecular system. The energy that then remains in the system may also lead to further fragmentation which, together with statistical fragmentation of heated intact molecules, gives the additional peaks in fig. 4.2.

Prompt knockout due to hard atom-atom scattering processes (nuclear stopping) does not only occur in collisions with He. In fig. 4.3 we see trajectories where one or more atoms have been removed from an anthracene ($C_{14}H_{10}$) molecule in MD simulations of atom-atom scattering in face-on collisions with noble gas atoms. The kinetic energies shown for the different gases in fig. 4.3 correspond to a constant collision velocity, $v = 0.034$ a.u., and the difference in energy is thus due to the difference in mass of the gas atoms. In this figure it is obvious that the cross section for knocking out one or more atoms from the molecule increases with target gas mass and nuclear charge. This picture is in good agreement with experimental results; the destruction cross section in these low velocity collisions is mainly driven by nuclear stopping. As seen in fig. 4.3, helium has a short range interaction compared to the heavier gases, and can thus more efficiently knock out an atom without heating up the rest of the molecule to the point where it will fragment further through secondary statistical processes.

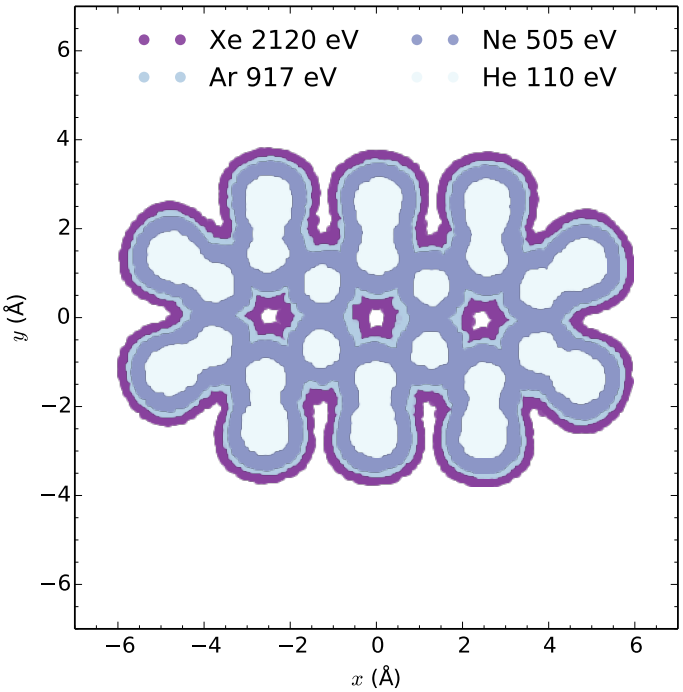

Figure 4.3: Trajectories, parallel to the z-axis, which result in the prompt knockout of atoms in MD simulations of face-on collisions between noble gas atoms and anthracene ($C_{14}H_{10}$) at a constant velocity, $v = 0.034$ a.u. The heavier gases interact at longer ranges due to their higher nuclear charge.

In order for non-statistical fragmentation to be observed directly, the large fragments following the knockout must be sufficiently cold to stay intact on the relevant experimental time scale, which here is of the order of tens of microseconds. This explains why the direct detection of C-loss from PAHs is so clear in low energy collisions with He. At higher collision energies, such as that shown in the lower panel of fig. 4.2, the electronic stopping, which deposits a large amount of energy to the whole molecule, becomes more important. So even though prompt knockout most likely occurs in such collisions, the direct evidence is lost in the subsequent fragmentation processes.

4.2.2 Molecular Clusters

The results of energy transfer in collisions between atoms and PAH or fullerene molecules can be expanded to the case with clusters of these molecules. The main difference here is that energy can not only be redistributed within a single molecule, but throughout the entire cluster [62–64]. Since the cluster has many more degrees of freedom than a single molecule, it can absorb more energy before reaching a given internal temperature. This has a stabilizing effect on the

molecules following keV collisions. Clusters also have the additional statistical fragmentation pathway of emitting intact molecules (binding energy up to about 1 eV [65–67]) as a means of cooling.

In Papers IV and V we used a simple Arrhenius type evaporation model to describe statistical dissociation of clusters of coronene or C_{60} molecules assuming sequential loss of single intact molecules [68]. The Arrhenius type evaporation rate Γ is given by $\Gamma = A\exp(-E_d/k_BT)$ where A is a pre-exponential factor, E_d the dissociation energy of the cluster - i.e. the binding energy of one molecule to the cluster, k_B Boltzmann's constant and T is the internal temperature of the cluster. The value of the pre-exponential factor has a relatively small effect on the total evaporation rate for our calculations and here we use $A = 10^{15}$ s^{-1} [63]. In Paper IV we assume that evaporation only occurs above a critical temperature T_{max}, the temperature for which the typical evaporation timescale surpasses the observation time ($t \approx 0.6$ μs in the experiments). The critical temperature can be estimated using $\Gamma_{max} \sim 1/t \Rightarrow T_{max} \approx \frac{E_d}{\ln(At)}$. The denominator in this expression is called the Gspann factor, $G = \ln(At)$. A typical value of $G = 23.5$ [68] for atomic and molecular cluster gives a critical temperature of about 150 K for cluster evaporation for C_{60} clusters ($E_d \approx 0.3$ eV) on the μs timescale.

The evaporation rate is driven by the the internal temperature of the cluster of size k, and the temperature of the remaining cluster becomes lower as the emitted molecule carries away internal energy and a finite kinetic and rotational energy. We used a semi-classical approach to determine the temperature as a function of the internal energy (that is, the heat capacity) for a given cluster size [68]. The intramolecular vibration modes were treated using the vibrational energies obtained from DFT calculations, while the rotation, translation and intermolecular modes were treated classically. Using this model, the internal energy per molecule in a cluster is given by

$$\frac{E_{\text{tot}}^{\text{vib}}}{k} = \sum_{i=1}^{3N-6} \frac{\hbar\omega_i}{\exp(\hbar\omega_i/k_BT_k) - 1} + \frac{k-1}{k} 6k_BT_k \tag{4.1}$$

where N is the number of atoms in a single molecule, ω_i is the frequency of the ith intramolecular vibration mode, and $\hbar$ is the reduced Planck constant. When a molecule is lost from the cluster, the energy lost is the internal energy of the molecule, the binding energy of that molecule and the average rotational and translation energy of a single molecule in the cluster ($6/2k_BT$), which give the recursive expression

$$E_{\text{tot}}^{\text{vib}}(k-1) = [1 - 1/k]\left[E_{\text{tot}}^{\text{vib}}(k) - (6/2)k_BT_k - E_d(k)\right] \tag{4.2}$$

for $2 \leq j \leq k$.

Calculating the vibrational levels of a single molecule is rather straightforward. For the countless number of cluster conformations, the fully harmonic approach (from DFT calculations) is impossible for all but the smallest clusters. Also, given the simplicity of the evaporation model in general, there is little to gain in using a more accurate description of the heat capacity. In fig. 4.4 the internal energy as a function of temperature for an anthracene dimer ($[C_{14}H_{10}]_2$) is shown for different descriptions of the internal energy. We see that the difference between the semi-classical approach and the full harmonic approach is negligible ($< 1\%$) for this small system. Despite the simplicity of the evaporation model, it does give a good qualitative description of the evaporation process of PAH and fullerene clusters (as shown in Paper V for coronene).

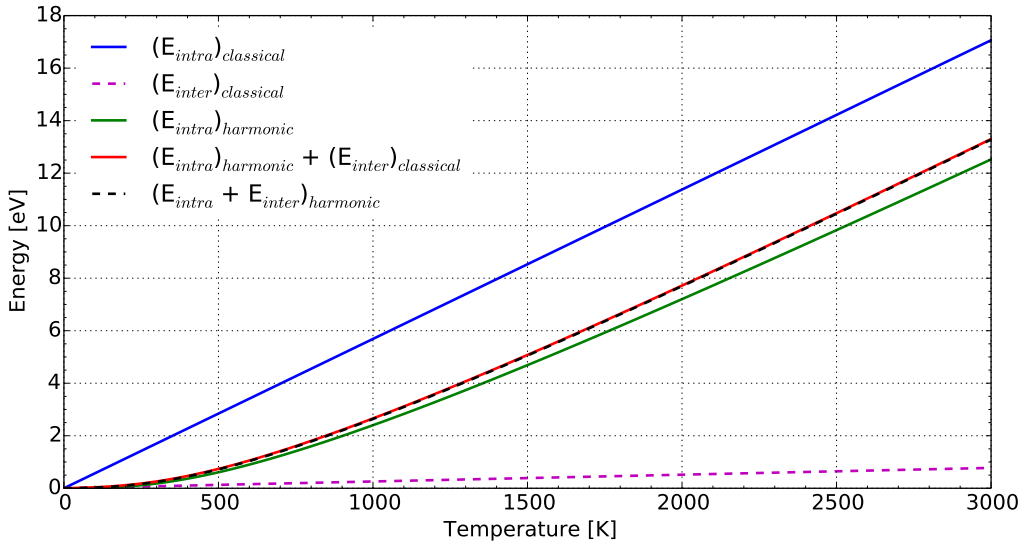

Figure 4.4: Internal energy as a function of temperature for an anthracene dimer calculated using different methods. The fully classic intramolecular energy is for two isolated molecules. The red curve is the sum of harmonic intramolecular energy (green curve) and the classical intermolecular energy (dashed pink curve). The semi-classical (red curve) and fully harmonic (dashed black curve) energies agree to within less than one percent.

Figure 4.5 shows a mass spectrum for collisions between 22.5 keV He^{2+} and clusters of a loosely bound mix of C_{60} and coronene ($C_{24}H_{12}$). The labeling used in the figure indicates the number of C_{60}, j, and the number of coronene, k, for a given peak with the form $[j,k]^+$. This mass spectrum has characteristics typical for evaporating clusters; the spectrum is dominated by the monomer peak and there are signs of ongoing evaporation in the right wings of some peaks (those labeled $[0,4]^+$ and $[0,5]^+$ for instance). The evaporation sequences are influenced by the types of molecules in the cluster. Fullerene clusters, while having lower binding energies than typical PAH clusters, tend to be more stable when heated in collisions due to the larger number of internal degrees of freedom of the fullerene molecule [33]. An interesting result from Paper VI is that the addition of a C_{60} molecule to a coronene cluster has a stabilizing effect, and now the cluster behaves more like a pure C_{60} cluster than one only containing coronene molecules.

4.3 Knockout Induced Chemistry

A subtle yet striking feature of the mass-to-charge spectrum resulting from collisions between 22.5 keV He^{2+} ions and mixed clusters containing C_{60} and coronene molecules with the average mixing factor of 1:3 is shown in the inset of fig. 4.5. In the region where one finds the C_{60} dimer, a result of evaporation of larger clusters or intact ionized dimers, the strongest feature is not the peak at 1440 amu, but a peak at mass 1428 amu corresponding to the mass of 119 carbon atoms. In experiments with clusters containing larger amounts of C_{60} or with pure C_{60} clusters this feature become even more prominent (Papers I, III, IV and VI). The detection of this

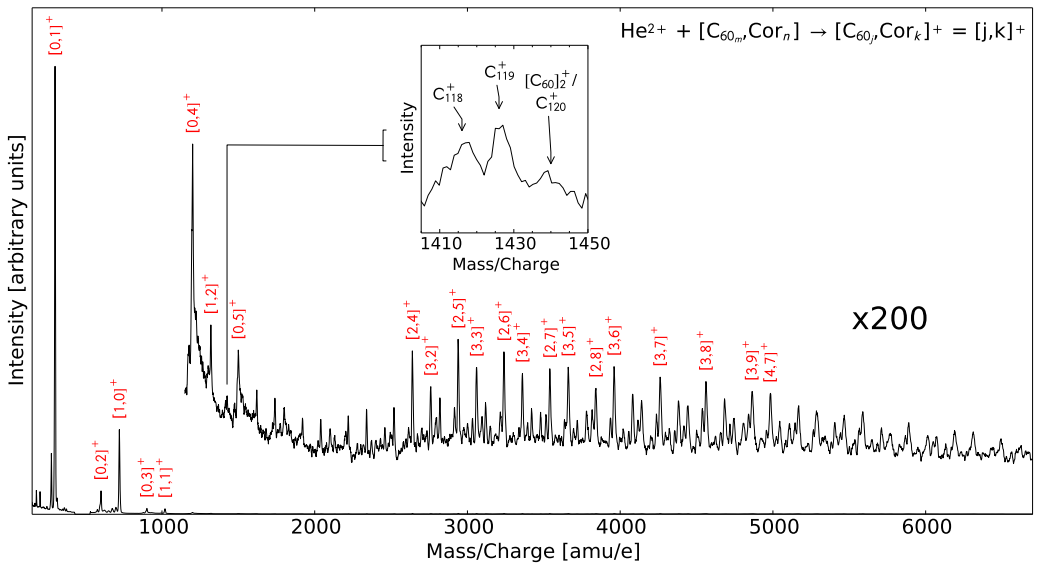

Figure 4.5: Mass spectrum from collisions between 22.5 keV He^{2+} ions and mixed clusters of C_{60} and coronene ($C_{24}H_{12}$). The spectrum shown here is the coronene-dominated spectrum mentioned in Paper VI. The strongest features in the mass spectrum are labelled with the number of molecules of each type. The inset shows the C^+_{119} and C^+_{118} which result from reactions following the knockout of one or two carbon atoms respectively.

peak clearly does not agree with the picture of statistical fragmentation of fullerene molecules or clusters. Only fullerenes containing an even number of carbon atoms are expected to be formed from statistical processes [60]. Instead, the C_{119} species is a result of non-statistical fragmentation through the knockout of a single C atom from a C_{60}, creating with C_{59} which then reacts with a neighboring C_{60} to form C_{119}.

The cluster environment is crucial for the survival of these comparatively fragile odd-numbered fullerene fragments (C_{59}) before they have a chance to collide with other molecules in the cluster. The isolated C_{59} fragment has only been observed in a few experiments at lower collision energies where nuclear stopping is dominant and the fragment remains cold enough to be detected ([35, 36, 69] and in Paper I). At center-of-mass collision energies above 20 keV, like the ones where C_{119} is detected, the electronic stopping is much higher and any isolated C_{59} molecule would rapidly fragment further. In the cluster environment however, the energy is redistributed throughout the cluster [62, 70] and the highly reactive C_{59} resists further fragmentation by forming covalent bonds with a neighboring intact C_{60} molecule.

Using MD and DFT calculations we have found that the $C_{59} + C_{60} \rightarrow C_{119}$ reaction is very efficient at collision energies up to 1 eV, that it is practically barrier-less, and that the C^+_{119} binding energy is about 5 eV (Papers III and IV). Figure 4.6 shows the results from an MD simulation of 1000 randomly oriented collisions between C_{59} and C_{60} at 0.8 eV center-of-mass energy, a typical value for collisions in dissociating clusters (Papers III, IV and VI). The figure

shows the number of simulations which result in a specific spatial separation between the two molecules which does not increase with time and therefore indicates the formation of covalent bonds. In this setup, most orientations lead to the two molecules bouncing off of each other without forming bonds. Bond formation occurs when the reactive site of C_{59} (the former position of the missing C atom) is located near the point of impact. With the appropriate orientation, the C_{59} and C_{60} efficiently form bonds, as seen from the peak near the inter-molecular separation of 7 Å. The resulting structure of C_{119} is the dumb-bell shaped molecule which is shown in Papers III, IV and VI.

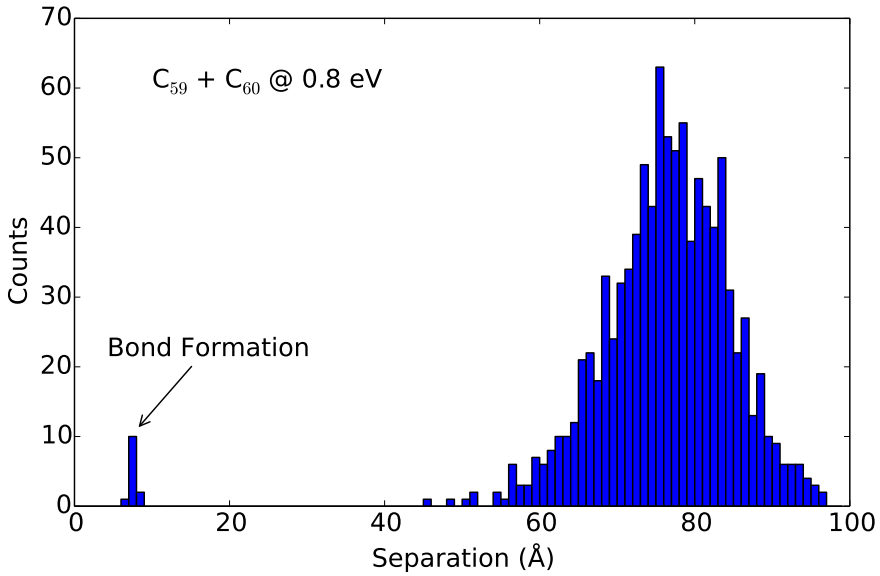

Figure 4.6: Separation between the centers of a C_{59} and C_{60} pair colliding with a center-of-mass energy of 0.8 eV from the present MD-simulations (i.e after 5 ps). Most collisions lead to the molecules bouncing off each other, but with the correct orientation covalent bonds may form. Bond formation is clearly identified by the peak at a separation of ~ 7 Å.

While we observe knockout induced fusion products in the mixed cluster experiments, the only such species detected is C_{119} (and C_{118} which is likely formed in a similar process) while no bond-formations are observed between fragmented C_{60} and intact coronene, between intact C_{60} and fragmented coronene or between fragments of both molecules. This even though the probability to knock out a single carbon atom from an isolated PAH molecule has been measured to be large (Paper II). In our MD simulations we found that C_{59} does not form bonds with coronene for typical molecule-molecule collision energies which we measure for our dissociating clusters. Only in the case of a single C-atom removed from the inner ring of coronene, do we find any appreciable reactivity with C_{60} below 1 eV. Still, our simulations indicate that this reaction probability is a factor of about 50 lower than the one for C_{59}+$C_{60} \rightarrow C_{119}$. A proposed molecular structure for the covalent product of $C_{23}H_{12}$+C_{60} is shown in fig. 4.7 (the C-atom initially removed from coronene was from its central hexagon).

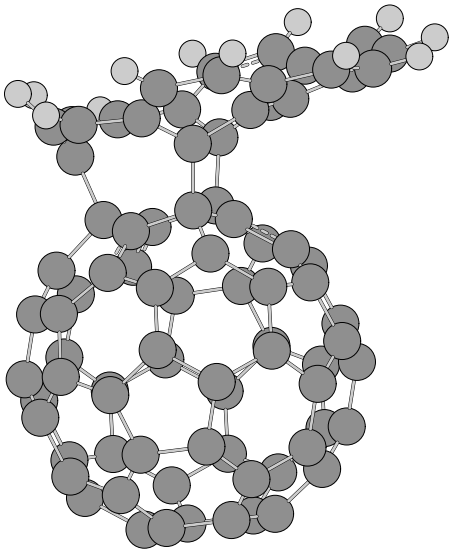

Figure 4.7: A reaction product observed in our MD-simulations of collisions between $C_{23}H_{12}$ (coronene missing a C atom) and C_{60} at a center-of-mass energy below 1 eV.

The knockout process could also accelerate PAH and fullerene growth in environments such as the interstellar medium. In Paper VII we showed that the reactivity of neutral and singly charged circumcoronene ($C_{54}H_{18}$) with astrophysically relevant molecules and atoms is greatly enhanced when a C atom is removed from the molecule. Since the thermal stability of PAHs increases with size, a large PAH such as circumcoronene is more likely to survive the initial collision than the smaller PAHs studied experimentally.

5. Summary and Outlook

In this thesis I have presented experimental and theoretical studies of collision induced dissociation of fullerenes, PAHs and clusters of these molecules. We have developed a model for calculating electronic and nuclear stopping energy for center-of-mass collision energies ranging from a few tens of eV and up to tens of keV. With this model we have shown that nuclear stopping is the dominant energy transfer mechanism in low energy collisions while electronic stopping dominates at higher collision energies. These differences are observed in the experiments through different fragmentation pathways for low and high collision energies.

Statistical fragmentation of molecules and clusters occurs when the energy deposited in a collision is redistributed over the entire system. The molecule or cluster will then usually fragment through the channels with the lowest dissociation energies. In the case of fullerene molecules this is through C_2 emission and for PAH molecules it is through C_2H_2 or H loss.

In short range interactions between two colliding nuclei, the energy transfer may be large. In such collisions, a large amount of energy may be transferred to a single atom in the system so that it is promptly knocked out of the molecule on timescales of the order of femtoseconds. Such a process is known as non-statistical fragmentation as there is no time to distribute the excitation energy over the whole molecular system before one or several atoms are removed. In the present studies the corresponding fragmentation pathways have high dissociation energies and are normally not observed in statistical decays. We have further seen that non-statistical fragmentation can lead to highly reactive species which can bond with neighboring molecules to form exotic new species such as C_{119} or $C_{53}H_{18}N$. This knockout driven reaction mechanism could play a role in an interstellar environment where stellar winds or plasma shocks can interact with fullerenes, PAHs, or clusters of these molecules.

A next step is to study these processes on timescales longer than a few microseconds. For this we will need to trap the molecules or their fragments in an ion trap or storage ring. Work is underway to prepare a new version of a simple linear electrostatic ion trap, ConeTrap [71], for the study of fragments of fullerene or PAH molecules after knockout collisions. Other options involve the possibilities made available by the DESIREE dual storage ring facility.

Construction of the Double ElectroStatic Ion Ring ExpEriment, DESIREE, at Stockholm University is complete and the first experiments are underway (Papers VIII and IX). DESIREE is a novel experiment with two 8.6 meter circumference electrostatic storage rings for keV ions (fig. 5.1). The two rings share a common straight merging section where oppositely charged ions can interact with controlled collision energies down to a few meV. The two storage rings are enclosed in a common vacuum vessel at a temperature which can be controlled down to about 11 K. This gives a very low residual gas density of about 10^4 cm^{-3} (equivalent to a pressure of about 10^{-14} mbar at 11 K).

The conditions in DESIREE allow for very long storage times, 11 minutes has for example

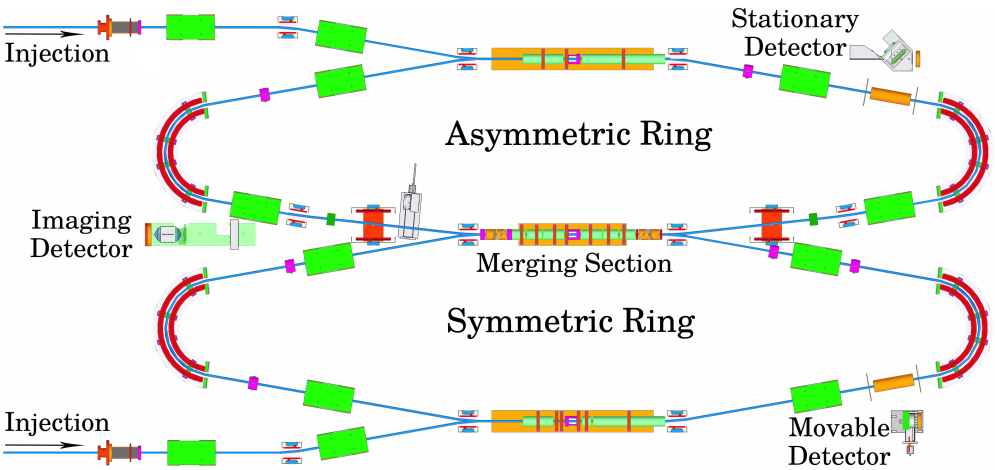

Figure 5.1: Overview of the DESIREE storage rings. The layout of the two rings are different from each other to allow for the simultaneous storage of ions with different mass-to-charge ratios (the heavier ions are stored in the asymmetric ring).

been measured as the $1/e$ lifetime of a 10 keV O^- beam. This, combined with the cryogenic temperatures, allow IR-active ions to cool to their ground states, giving well defined conditions for experiments. As a result of DESIREE's unique characteristics, we are able to accurately study fundamental reactions in the gas phase down to very low relative energies. Examples of mechanisms that can be studied include mutual neutralization of oppositely charged ions, reaction barriers and inherent lifetimes of loosely bound states such as excited anions.

The first experiments in DESIREE involve atomic and small molecular systems such as studies of the metastable excited state of C^- and the mutual neutralization in $C^+ + C^-$ and $H^+ + H^-$ collisions. Experiments involving fullerenes, PAHs, and atomic clusters are planned as well.

Additional Publications

The following peer-reviewed papers and conference contributions were not included in this thesis.

Disc scalelengths out to redshift 5.8
K. Fathi, M. Gatchell, E. Hatziminaoglou and B. Epinat, *Monthly Notices of the Royal Astronomical Society Letters*, **423**, L112 (2012).
DOI: 10.1111/j.1745-3933.2012.01270.x

Ionization and fragmentation of cold clusters of PAH molecules - collisions with keV ions
A. I. S. Holm, H. Zettergren, M. Gatchell, H. A. B. Johansson, F. Seitz, H. T. Schmidt, P. Rousseau, A. Ławicki, M. Capron, A. Domaracka, E. Lattouf, S. Maclot, R. Maisonny, J.-Y. Chesnel, B. Manil, L. Adoui, B. A. Huber, and H. Cederquist, *Journal of Physics: Conference Series*, **388**, 012051 (2012).
DOI: 10.1088/1742-6596/388/1/012051

Ions interacting with planar aromatic molecules: Modeling electron transfer reactions
B. O. Forsberg, J. D. Alexander, T. Chen, A. T. Pettersson, M. Gatchell, H. Cederquist, and H. Zettergren, *The Journal of Chemical Physics*, **138**, 054306 (2012).
DOI: 10.1063/1.4790164

Bond formation in C_{59}^+ - C_{60} collisions
H. Zettergren, P. Rousseau, Y. Wang, F. Seitz, T. Chen, M. Gatchell, J. D. Alexander, M. H. Stockett, J. Rangama, J. Y. Chesnel, M. Capron, J. C. Poully, A. Domaracka, A. Méry, S. Maclot, V. Vizcaino, H. T. Schmidt, L. Adoui, M. Alcamí, A. G. G. M. Tielens, F. Martín, B. A. Huber, and H. Cederquist, *Journal of Physics: Conference Series*, **488**, 012028 (2014).
DOI: 10.1088/1742-6596/488/1/012028

Formation dynamics of fullerene dimers C_{118}^+, C_{119}^+ and C_{120}^+
Y. Wang, H. Zettergren, P. Rousseau, T. Chen, M. Gatchell, M. H. Stockett, A. Domaracka, L. Adoui, B. A. Huber, H. Cederquist, M. Alcamí, and F. Martín, *Physical Review A*, accepted (2014).

References

[1] A. G. G. M. TIELENS. **The molecular universe**. *Rev. Mod. Phys.*, **85**:1021–1081, Jul 2013. 11

[2] WILLIAM KLEMPERER. **Astronomical Chemistry**. *Annual Review of Physical Chemistry*, **62**(1):173–184, 2011. PMID: 21128763. 11

[3] A. LEGER AND J. L. PUGET. **Identification of the 'unidentified' IR emission features of interstellar dust?** *Astronomy and Astrophysics*, **137**:L5–L8, August 1984. 11

[4] A.G.G.M. TIELENS. **Interstellar Polycyclic Aromatic Hydrocarbon Molecules***. *Annual Review of Astronomy and Astrophysics*, **46**(1):289–337, 2008. 11

[5] MATTHEW S. POVICH, JENNIFER M. STONE, ED CHURCHWELL, ELLEN G. ZWEIBEL, MARK G. WOLFIRE, BRIAN L. BABLER, RÉMY INDEBETOUW, MARILYN R. MEADE, AND BARBARA A. WHITNEY. **A Multiwavelength Study of M17: The Spectral Energy Distribution and PAH Emission Morphology of a Massive Star Formation Region**. *The Astrophysical Journal*, **660**(1):346, 2007. 11

[6] M. RAPACIOLI, C. JOBLIN, AND P. BOISSEL. **Spectroscopy of polycyclic aromatic hydrocarbons and very small grains in photodissociation regions**. *Astronomy and Astrophysics*, **429**(1):193–204, 2005. 11

[7] S. DRAPATZ S.K. GHOSH. **Very Small Grains in Spiral Galaxies**. In D'HENDECOURT LÉGER AND BOCCARA, editors, *Polycyclic Aromatic Hydrocarbons and Astrophysics*, NATO ASI Series, pages 317–322. D. Reidel, 1987.

[8] E. PEETERS, S. HONY, C. VAN KERCKHOVEN, A. G. G. M. TIELENS, L. J. ALLAMANDOLA, D. M. HUDGINS, AND C. W. BAUSCHLICHER. **The rich 6 to 9 μm spectrum of interstellar PAHs**. *A&A*, **390**(3):1089–1113, 2002. 11

[9] B.T. DRAINE. **INTERSTELLAR DUST GRAINS**. *Annual Review of Astronomy and Astrophysics*, **41**(1):241–289, 2003. 11

[10] H. W. KROTO, J. R. HEATH, S. C. O'BRIEN, R. F. CURL, AND R. E. SMALLEY. **C60: Buckminsterfullerene**. *Nature*, **318**(6042):162–163, 11 1985. 11

[11] KRIS SELLGREN, MICHAEL W. WERNER, JAMES G. INGALLS, J. D. T. SMITH, T. M. CARLETON, AND CHRISTINE JOBLIN. **C60 in Reflection Nebulae**. *The Astrophysical Journal Letters*, **722**(1):L54, 2010. 11

[12] JAN CAMI, JERONIMO BERNARD-SALAS, ELS PEETERS, AND SARAH ELIZABETH MALEK. **Detection of C60 and C70 in a Young Planetary Nebula**. *Science*, **329**(5996):1180–1182, 2010.

[13] D. A. GARCÍA-HERNÁNDEZ, A. MANCHADO, P. GARCÍA-LARIO, L. STANGHELLINI, E. VILLAVER, R. A. SHAW, R. SZCZERBA, AND J. V. PEREA-CALDERÓN. **Formation of Fullerenes in H-containing Planetary Nebulae**. *The Astrophysical Journal Letters*, **724**(1):L39, 2010.

[14] D. A. GARCÍA-HERNÁNDEZ, S. IGLESIAS-GROTH, J. A. ACOSTA-PULIDO, A. MANCHADO, P. GARCÍA-LARIO, L. STANGHELLINI, E. VILLAVER, R. A. SHAW, AND F. CATALDO. **The Formation of Fullerenes: Clues from New C60, C70, and (Possible) Planar C24 Detections in Magellanic Cloud Planetary Nebulae**. *The Astrophysical Journal Letters*, **737**(2):L30, 2011. 11

[15] OLIVIER BERNÉ AND A. G. G. M. TIELENS. **Formation of buckminsterfullerene (C60) in interstellar space**. *Proceedings of the National Academy of Sciences*, **109**(2):401–406, 01 2012. 11

[16] ELS PEETERS. **The PAH Hypothesis after 25 Years**. *Proceedings of the International Astronomical Union*, **7**:149–161, 6 2011. 11

[17] BIKAU SHUKLA AND MITSUO KOSHI. **Comparative study on the growth mechanisms of PAHs**. *Combustion and Flame*, **158**(2):369 – 375, 2011. 11

[18] PAUL W. DUNK, NATHAN K. KAISER, CHRISTOPHER L. HENDRICKSON, JOHN P. QUINN, CHRISTOPHER P. EWELS, YUSUKE NAKANISHI, YUKI SASAKI, HISANORI SHINOHARA, ALAN G. MARSHALL, AND HAROLD W. KROTO. **Closed network growth of fullerenes**. *Nat Commun*, **3**:855, 05 2012. 11

[19] JIANYUAN ZHANG, FAYE L. BOWLES, DANIEL W. BEARDEN, W. KEITH RAY, TIM FUHRER, YOUQING YE, CAITLYN DIXON, KIM HARICH, RICHARD F. HELM, MARILYN M. OLMSTEAD, ALAN L. BALCH, AND HARRY C. DORN. **A missing link in the transformation from asymmetric to symmetric metallofullerene cages implies a top-down fullerene formation mechanism**. *Nat Chem*, **5**(10):880–885, 10 2013. 11

[20] C. JOBLIN, A. LEGER, AND P. MARTIN. **Contribution of polycyclic aromatic hydrocarbon molecules to the interstellar extinction curve**. *Astrophysical Journal Letters*, **393**:L79–L82, July 1992. 12

[21] SCOTT P. EKERN, ALAN G. MARSHALL, JAN SZCZEPANSKI, AND MARTIN VALA. **Photodissociation of Gas-Phase Polycylic Aromatic Hydrocarbon Cations**. *The Journal of Physical Chemistry A*, **102**(20):3498–3504, 1998.

[22] H. W. JOCHIMS, E. RUHL, H. BAUMGARTEL, S. TOBITA, AND S. LEACH. **Size effects on dissociation rates of polycyclic aromatic hydrocarbon cations: Laboratory studies and astophysical implications**. *Astrophysical Journal*, **420**:307–317, January 1994.

[23] MASANAO MURAKAMI, RYUJI MIZOGUCHI, YOSHINORI SHIMADA, TOMOYUKI YATSUHASHI, AND NOBUAKI NAKASHIMA. **Ionization and fragmentation of anthracene with an intense femtosecond laser pulse at 1.4 μm**. *Chemical Physics Letters*, **403**(4–6):238 – 241, 2005.

[24] KLÆRKE, B., TOKER, Y., RAHBEK, D. B., HORNEKÆR, L., AND ANDERSEN, L. H. **Formation and stability of hydrogenated PAHs in the gas phase**. *A&A*, **549**:A84, 2013.

[25] S. MARTIN, J. BERNARD, R. BRÉDY, B. CONCINA, C. JOBLIN, M. JI, C. ORTEGA, AND L. CHEN. **Fast Radiative Cooling of Anthracene Observed in a Compact Electrostatic Storage Ring**. *Phys. Rev. Lett.*, **110**:063003, Feb 2013. 12

[26] P. SCHEIER AND T. D. MÄRK. **Observation of the Septuply Charged ion C_{60}^{7+} and Its Metastable Decay into Two Charged Fragments via Superasymmetric Fission**. *Phys. Rev. Lett.*, **73**:54–57, Jul 1994. 12

[27] S. TOMITA, H. LEBIUS, A. BRENAC, F. CHANDEZON, AND B. A. HUBER. **Energetics in charge-separation processes of highly charged fullerene ions**. *Phys. Rev. A*, **67**:063204, Jun 2003. 12

[28] A. ŁAWICKI, A. I. S. HOLM, P. ROUSSEAU, M. CAPRON, R. MAISONNY, S. MACLOT, F. SEITZ, H. A. B. JOHANSSON, S. ROSÉN, H. T. SCHMIDT, H. ZETTERGREN, B. MANIL, L. ADOUI, H. CEDERQUIST, AND B. A. HUBER. **Multiple ionization and fragmentation of isolated pyrene and coronene molecules in collision with ions**. *Phys. Rev. A*, **83**:022704, Feb 2011.

[29] J. POSTMA, S. BARI, R. HOEKSTRA, A. G. G. M. TIELENS, AND T. SCHLATHÖLTER. **Ionization and Fragmentation of Anthracene upon Interaction with keV Protons and α Particles**. *The Astrophysical Journal*, **708**(1):435, 2010. 25

[30] P. M. MISHRA, J. RAJPUT, C. P. SAFVAN, S. VIG, AND U. KADHANE. **Electron emission and electron transfer processes in proton-naphthalene collisions at intermediate velocities**. *Phys. Rev. A*, **88**:052707, Nov 2013.

[31] S. MARTIN, L. CHEN, R. BRÉDY, J. BERNARD, M. C. BUCHET-POULIZAC, A. ALLOUCHE, AND J. DÉSESQUELLES. **Emission of singly and doubly charged light fragments from $C_{60}^{r+}(r = 4-9)$ in $Xe^{25+} - C_{60}$ collisions**. *Phys. Rev. A*, **66**:063201, Dec 2002.

[32] G REITSMA, H ZETTERGREN, L BOSCHMAN, E BODEWITS, R HOEKSTRA, AND T SCHLATHÖLTER. **Ion–polycyclic aromatic hydrocarbon collisions: kinetic energy releases for specific fragmentation channels**. *Journal of Physics B: Atomic, Molecular and Optical Physics*, **46**(24):245201, 2013.

[33] B. MANIL, L. MAUNOURY, B. A. HUBER, J. JENSEN, H. T. SCHMIDT, H. ZETTERGREN, H. CEDERQUIST, S. TOMITA, AND P. HVELPLUND. **Highly Charged Clusters of Fullerenes: Charge Mobility and Appearance Sizes**. *Phys. Rev. Lett.*, **91**:215504, Nov 2003. 34

[34] A. I. S. HOLM, H. ZETTERGREN, H. A. B. JOHANSSON, F. SEITZ, S. ROSÉN, H. T. SCHMIDT, A. ŁAWICKI, J. RANGAMA, P. ROUSSEAU, M. CAPRON, R. MAISONNY, L. ADOUI, A. MÉRY, B. MANIL, B. A. HUBER, AND H. CEDERQUIST. **Ions Colliding with Cold Polycyclic Aromatic Hydrocarbon Clusters**. *Phys. Rev. Lett.*, **105**:213401, Nov 2010. 12

[35] M.C. LARSEN, P. HVELPLUND, M.O. LARSSON, AND H. SHEN. **Fragmentation of fast positive and negative C ions in collisions with rare gas atoms**. *The European Physical Journal D - Atomic, Molecular, Optical and Plasma Physics*, **5**(2):283–289, 1999. 12, 35

[36] S. TOMITA, P. HVELPLUND, S. B. NIELSEN, AND T. MURAMOTO. **C_{59}-ion formation in high-energy collisions between cold C_{60}^- and noble gases**. *Phys. Rev. A*, **65**:043201, Apr 2002. 12, 35

[37] H.J.G.L.M. LAMERS AND J.P. CASSINELLI. *Introduction to stellar winds*. Cambridge University Press, 1999. 12

[38] MICELOTTA, E. R., JONES, A. P., AND TIELENS, A. G. G. M. **Polycyclic aromatic hydrocarbon processing in interstellar shocks**. *A&A*, **510**:A36, 2010. 12

[39] T. BERGEN, X. BIQUARD, A. BRENAC, F. CHANDEZON, B. A. HUBER, D. JALABERT, H. LEBIUS, M. MAUREL, E. MONNAND, J. OPITZ, A. PESNELLE, B. PRAS, C. RISTORI, AND J. C. ROCCO. **Multiply charged cluster ion crossed-beam apparatus: Multi-ionization of clusters by ion impact**. *Review of Scientific Instruments*, **70**(8):3244–3253, 1999. 13

[40] JOCHEN MAUL, THOMAS BERG, EDIT MAROSITS, GERD SCHÖNHENSE, AND GERHARD HUBER. **Statistical mechanics of fullerene coalescence growth**. *Phys. Rev. B*, **74**:161406, Oct 2006. 13

[41] N. R. DALY. **High Sensitivity Mass Spectrometer Leak Detector**. *Review of Scientific Instruments*, **31**(7):720–723, 1960. 14

[42] A BRENAC, F CHANDEZON, H LEBIUS, A PESNELLE, S TOMITA, AND B A HUBER. **Multifragmentation of Highly Charged C 60 Ions: Charge States and Fragment Energies**. *Physica Scripta*, **1999**(T80B):195, 1999. 15

[43] R. D. THOMAS, H. T. SCHMIDT, G. ANDLER, M. BJORKHAGE, M. BLOM, L. BRANNHOLM, E. BACKSTROM, H. DANARED, S. DAS, N. HAAG, P. HALLDEN, F. HELLBERG, A. I. S. HOLM, H. A. B. JOHANSSON, A. KALLBERG, G. KALLERSJO, M. LARSSON, S. LEONTEIN, L. LILJEBY, P. LOFGREN, B. MALM, S. MANNERVIK, M. MASUDA, D. MISRA, A. ORBAN, A. PAAL, P. REINHED, K. G. RENSFELT, S. ROSEN, K. SCHMIDT, F. SEITZ, A. SIMONSSON, J. WEIMER, H. ZETTERGREN, AND H. CEDERQUIST. **The double electrostatic ion ring experiment: A unique cryogenic electrostatic storage ring for merged ion-beams studies**. *Review of Scientific Instruments*, **82**(6):065112, JUN 2011. 16

[44] MALCOLM DOLE, L. L. MACK, R. L. HINES, R. C. MOBLEY, L. D. FERGUSON, AND M. B. ALICE. **Molecular Beams of Macroions**. *The Journal of Chemical Physics*, **49**(5):2240–2249, 1968. 16

[45] KLAUS CAPELLE. **A bird's-eye view of density-functional theory**. *Brazilian Journal of Physics*, **36**:1318 – 1343, 12 2006. 20

[46] P. HOHENBERG AND W. KOHN. **Inhomogeneous Electron Gas**. *Phys. Rev.*, **136**:B864–B871, Nov 1964. 20

[47] AXEL D. BECKE. **Density-functional thermochemistry. III. The role of exact exchange**. *The Journal of Chemical Physics*, **98**(7):5648–5652, 1993. 20

[48] JENG-DA CHAI AND MARTIN HEAD-GORDON. **Long-range corrected hybrid density functionals with damped atom-atom dispersion corrections**. *Physical Chemistry Chemical Physics*, **10**(44):6615–6620, 2008. 20

[49] YAN ZHAO AND DONALD G. TRUHLAR. **A new local density functional for main-group thermochemistry, transition metal bonding, thermochemical kinetics, and noncovalent interactions**. *The Journal of Chemical Physics*, **125**(19):–, 2006. 20

[50] STEFAN GRIMME. **Density functional theory with London dispersion corrections**. *Wiley Interdisciplinary Reviews: Computational Molecular Science*, **1**(2):211–228, 2011. 20

[51] J. TERSOFF. **New empirical approach for the structure and energy of covalent systems**. *Phys. Rev. B*, **37**:6991–7000, Apr 1988. 22

[52] J. TERSOFF. **Modeling solid-state chemistry: Interatomic potentials for multicomponent systems**. *Phys. Rev. B*, **39**:5566–5568, Mar 1989. 22, 23

[53] F. de Brito Mota, J. F. Justo, and A. Fazzio. **Hydrogen role on the properties of amorphous silicon nitride**. *Journal of Applied Physics*, **86**(4):1843–1847, 1999. 23

[54] J. Postma, R. Hoekstra, A. G. G. M. Tielens, and T. Schlathölter. **A Molecular Dynamics Study on Slow Ion Interactions with the Polycyclic Aromatic Hydrocarbon Molecule Anthracene**. *The Astrophysical Journal*, **783**(1):61, 2014. 23

[55] W. Smith and T.R. Forester. **DL_POLY_2.0: A general-purpose parallel molecular dynamics simulation package**. *Journal of Molecular Graphics*, **14**(3):136 – 141, 1996. 23

[56] Jacek Jakowski, Stephan Irle, and Keiji Morokuma. **Collision-induced fusion of two C_{60} fullerenes: Quantum chemical molecular dynamics simulations**. *Phys. Rev. B*, **82**:125443, Sep 2010. 24

[57] T. L. Ferrell and R. H. Ritchie. **Energy losses by slow ions and atoms to electronic excitation in solids**. *Phys. Rev. B*, **16**:115–123, Jul 1977. 25

[58] M. J. Puska and R. M. Nieminen. **Atoms embedded in an electron gas: Phase shifts and cross sections**. *Phys. Rev. B*, **27**:6121–6128, May 1983. 26

[59] S. Martin, L. Chen, R. Brédy, G. Montagne, C. Ortega, T. Schlathölter, G. Reitsma, and J. Bernard. **Statistical fragmentation of doubly charged anthracene induced by fluorine-beam impact at 3 keV**. *Phys. Rev. A*, **85**:052715, May 2012. 29

[60] S. Tomita, J. U. Andersen, C. Gottrup, P. Hvelplund, and U. V. Pedersen. **Dissociation Energy for C_2 Loss from Fullerene Cations in a Storage Ring**. *Phys. Rev. Lett.*, **87**:073401, Jul 2001. 30, 35

[61] A. I. S. Holm, H. A. B. Johansson, H. Cederquist, and H. Zettergren. **Dissociation and multiple ionization energies for five polycyclic aromatic hydrocarbon molecules**. *The Journal of Chemical Physics*, **134**(4):–, 2011. 30

[62] Henning Zettergren, Henning T. Schmidt, Peter Reinhed, Henrik Cederquist, Jens Jensen, Preben Hvelplund, Shigeo Tomita, Bruno Manil, Jimmy Rangama, and Bernd A. Huber. **Stabilities of multiply charged dimers and clusters of fullerenes**. *The Journal of Chemical Physics*, **126**(22):–, 2007. 32, 35

[63] H. A. B. Johansson, H. Zettergren, A. I. S. Holm, F. Seitz, H. T. Schmidt, P. Rousseau, A. Ławicki, M. Capron, A. Domaracka, E. Lattouf, S. Maclot, R. Maisonny, B. Manil, J.-Y. Chesnel, L. Adoui, B. A. Huber, and H. Cederquist. **Ionization and fragmentation of polycyclic aromatic hydrocarbon clusters in collisions with keV ions**. *Phys. Rev. A*, **84**:043201, Oct 2011. 33

[64] A I S Holm, H Zettergren, M Gatchell, H A B Johansson, F Seitz, H T Schmidt, P Rousseau, A Ławicki, M Capron, A Domaracka, E Lattouf, S Maclot, R Maisonny, J-Y Chesnel, B Manil, L Adoui, B A Huber, and H Cederquist. **Ionization and fragmentation of cold clusters of PAH molecules – collisions with keV ions**. *Journal of Physics: Conference Series*, **388**(1):012051, 2012. 32

[65] T. P. Martin, U. Näher, H. Schaber, and U. Zimmermann. **Clusters of fullerene molecules**. *Phys. Rev. Lett.*, **70**:3079–3082, May 1993. 33

[66] M. Rapacioli, F. Calvo, F. Spiegelman, C. Joblin, and D. J. Wales. **Stacked Clusters of Polycyclic Aromatic Hydrocarbon Molecules**. *The Journal of Physical Chemistry A*, **109**(11):2487–2497, 2005.

[67] M. Rapacioli and F. Spiegelman. **Modelling singly ionized coronene clusters**. *The European Physical Journal D*, **52**(1-3):55–58, 2009. 33

[68] Martin Schmidt, Albert Masson, and Catherine Bréchignac. **Coronene cluster experiments: Stability and thermodynamics**. *International Journal of Mass Spectrometry*, **252**(2):173 – 179, 2006. Special Issue on Cluster Cooling. 33

[69] James F. Christian, Zhimin Wan, and Scott L. Anderson. **Nitrogen ion (N+) + C60 fullerene reactive scattering: substitution, charge transfer, and fragmentation**. *The Journal of Physical Chemistry*, **96**(26):10597–10600, 1992. 35

[70] Henning Zettergren, Yang Wang, Al Mokhtar Lamsabhi, Manuel Alcamí, and Fernando Martín. **Density functional theory study of multiply ionized weakly bound fullerene dimers**. *The Journal of Chemical Physics*, **130**(22):–, 2009. 35

[71] Henning T. Schmidt, Henrik Cederquist, Jens Jensen, and Afshin Fardi. **Conetrap: A compact electrostatic ion trap**. *Nuclear Instruments and Methods in Physics Research Section B: Beam Interactions with Materials and Atoms*, **173**(4):523 – 527, 2001. 39